RESEARCH ARTICLE

Anoctamin Calcium-Activated Chloride Channels May Modulate Inhibitory Transmission in the Cerebellar Cortex

Weiping Zhang[☉], Steffen Schmelzeisen[☉], Daniel Parthier, Stephan Frings, Frank Möhrlen*

Department of Animal Molecular Physiology, Centre of Organismal Studies, Im Neuenheimer Feld 504, Heidelberg University, Heidelberg, Germany

☉ These authors contributed equally to this work.
* moehrlen@uni-hd.de

Abstract

Calcium-activated chloride channels of the anoctamin (alias TMEM16) protein family fulfill critical functions in epithelial fluid transport, smooth muscle contraction and sensory signal processing. Little is known, however, about their contribution to information processing in the central nervous system. Here we examined the recent finding that a calcium-dependent chloride conductance impacts on GABAergic synaptic inhibition in Purkinje cells of the cerebellum. We asked whether anoctamin channels may underlie this chloride conductance. We identified two anoctamin channel proteins, ANO1 and ANO2, in the cerebellar cortex. ANO1 was expressed in inhibitory interneurons of the molecular layer and the granule cell layer. Both channels were expressed in Purkinje cells but, while ANO1 appeared to be retained in the cell body, ANO2 was targeted to the dendritic tree. Functional studies confirmed that ANO2 was involved in a calcium-dependent mode of ionic plasticity that reduces the efficacy of GABAergic synapses. ANO2 channels attenuated GABAergic transmission by increasing the postsynaptic chloride concentration, hence reducing the driving force for chloride influx. Our data suggest that ANO2 channels are involved in a Ca^{2+}-dependent regulation of synaptic weight in GABAergic inhibition. Thus, in balance with the chloride extrusion mechanism via the co-transporter KCC2, ANO2 appears to regulate ionic plasticity in the cerebellum.

Introduction

Calcium-activated chloride channels of the anoctamin (alias TMEM16) family of membrane proteins provide a chloride conductance that operates under the control of intracellular Ca^{2+} signals (recent review: [1]). Many different cell types express anoctamin proteins. The anoctamin chloride channels anoctamin 1 (ANO1, TMEM16A) and anoctamin 2 (ANO2, TMEM16B) have been established as Ca^{2+}-activated Cl^- channels with defined physiological functions [2–4]. They are involved in epithelial Cl^- transport, smooth muscle contraction and neuronal signal processing. Anoctamin channels show highly polarized expression patterns in

epithelia and neurons, making spatial aspects crucial for understanding channel function. Moreover, ANO1 and ANO2 display a ten-fold difference in Ca^{2+} sensitivity, and various splice forms of these proteins respond to different Ca^{2+} levels [5,6]. Finally, the channels may conduct Cl^- influx or Cl^- efflux, the balance being decided by the dynamic system of intracellular chloride regulation that includes various Cl^-/cation co-transporters and their regulatory proteins.

There is a surprising paucity of data on ANO1 and ANO2 in the central nervous system. So far, most of the published data on neuronal expression concern sensory systems. The channels are localized in the chemosensory cilia of olfactory receptor neurons [7–11], in vomeronasal sensory neurons [8,12,13], in rod photoreceptor synaptic terminals [8,14–16], at the cochlear hair-cell synapse, and in the auditory brainstem [17–19], as well as in neurons of the dorsal root ganglia and trigeminal ganglia where they contribute to the processing of heat nociception and inflammatory hyperalgesia [20–25]. Thus, anoctamin chloride channels are clearly involved in the generation, modulation and synaptic transmission of sensory signals. However, based on mRNA expression, there is evidence that the channels are also expressed in various parts of the brain [18,26,27]. But, apart from a proposed epithelial function in the choroid plexus [28] and myogenic effects in cerebral arteries [29,30], there is to our knowledge only one concept for anoctamin-channel function in neuronal networks. In hippocampal neurons, ANO2 appears to influence the efficacy of action potential generation by providing a Ca^{2+}-regulated shunt conductance in dendrites, which attenuates output activity [27].

Here we report evidence for a further possible role of anoctamin channels in the brain: the regulation of ionic plasticity of GABAergic synapses in the cerebellar cortex. It was recently reported that cerebellar Purkinje cells use Ca^{2+}-activated Cl^- channels to modulate the efficacy of synaptic input from inhibitory interneurons, a process termed *depolarization-induced depression of inhibition* (*DDI*) [31]. We carried out expression studies and electrophysiological tests to find out whether the Ca^{2+}-activated Cl^- channels that mediate *DDI* may be formed by anoctamin proteins. We report that both ANO1 and ANO2 are expressed in the murine cerebellar cortex. The channels display a differential expression pattern. ANO1 is mainly expressed in inhibitory interneurons and in Purkinje cell somata. In contrast, ANO2 is expressed only in Purkinje cells where it is targeted to the dendritic tree. Functional studies revealed that the modulatory effect reported by Satoh *et al.* (2103) [31] is absent in $Ano2^{-/-}$ mice. Our results point to distinct functions of ANO1 and ANO2 in the cerebellar cortex. ANO1 appears to be a component in the network of inhibitory interneurons, while ANO2 may modulate the inhibitory input to Purkinje cells.

Materials and Methods

Animals

4 to 20-week-old male C57BL/6 (Black6) mice and $Ano2^{-/-}$ mice [8], kindly provided by Dr. Thomas Jentsch (Leipniz-Institute for Molecular Pharmacology, Berlin), were used for the experiments. GAD^{Cre} mice [32] were kindly provided by Dr. Hannah Monyer (Heidelberg University). Animals were anesthetized and killed by an overdose of isoflurane (Baxter, Germany). All experiments were performed in accordance with the Animal Protection Law and the guidelines and permissions of Heidelberg University.

Immunohistochemistry

Unfixed fresh mouse brains were embedded in tissue freezing medium (Leica Biosystems) and sliced in a cryotome (Leica CM 3050S). 20 μm thick cryosections were fixed with 2% PFA for 15 minutes, washed 3×5 minutes with PBS (130 mM NaCl, 8.1 mM Na_2HPO_4, 1.9 mM NaH_2PO_4, pH 7.4), and were subsequently processed for staining. DAB-staining was

performed using the Vectastain ABC kit guinea pig IgG (biotinylated secondary antibody dilution 1:200; PK-4007; Vector Labs). Sections were incubated in 0.5% H_2O_2 for 1 hour and washed 3×5 minutes with PBS, followed by incubation in blocking solution (5% normal goat serum, Sigma-Aldrich, G9023, in PBS with 0.5% Triton X-100, 0.05% NaN_3) for 1 hour. The primary antiserum was diluted in blocking solution and applied overnight at 4°C, then washed for 3×10 minutes with PBS. Sections were then incubated in biotinylated secondary antibodies, diluted in blocking solution, for 2 hours, washed 3×10 minutes in PBS, incubated in ABC solution (from the ABC Kit, one drop of A and one drop of B in 20 ml PBS, prepared at least 30 minutes before use) for 1 hour, and washed 3×10 minutes with PBS. Sections were developed for 5 minutes with DAB-H_2O_2 solution (1µl of 1% H_2O_2 in 1 ml 3,3'-diaminobenzidin solution; one pellet DAB in 10 ml PBS; Sigma-Aldrich D5905) to start the reaction, washed with PBS intensively, and mounted on glass slides using Aqua-Poly/Mount (Polysciences, Inc., 18606). For immunofluorescence staining, sections were incubated by blocking serum for 1 hour, and the primary antisera (diluted in blocking solution) were applied overnight at 4°C for brains, and 2 hours at room temperature for noses. After washing 3 x 10 min with PBS, the secondary antisera, conjugated with Alexa Fluor tags (Molecular Probes, Inc.), were incubated for 2 hours, washed 3 x 10 minutes with PBS. To visualize cell nuclei, the slices were incubated in DAPI (0.3 µM 4,6-diamidin-2-phenylindol in PBS; Sigma-Aldrich 32670) for 3 minutes, washed 3 x 5 minutes in PBS and mounted on glass slides with Aqua-Poly/Mount. To stain all neurons, we incubated sections in NeuroTrace[®] 530/615 (Invitrogen N21482, dilution 1:500; Life Technologies, Inc.) for 5 minutes before the DAPI treatment, followed by 3 x 5 minutes wash with PBS. Images were obtained using a Nikon C1 confocal microscope. All imaging data presented are single-plane images, no Z-stacks are used in this paper.

Primary antisera for ANO1 were raised in guinea pig against the intracellular C-terminus ("ANO1$_{in}$" in the text, dilution 1:200, [33]) and in rabbit against the extracellular loop between transmembrane domains 9 and 10 ("ANO1$_{ex}$", dilution 1:250, Alomone Labs, ACL011). Both ANO1 antisera showed the same specific staining patterns in our positive controls (nasal epithelia). The primary antiserum against ANO2 ("ANO2$_{in}$" in the text) was raised in guinea pig against the intracellular loop connecting transmembrane domains 2 and 3 (dilution 1:200; [33]) and was characterized in previous publications [12,26,33]. To verify the specificity of the ANO antisera, we used cryosections of the mouse vomeronasal organ (VNO) because the sensory neurons in the VNO express both ANO1 and ANO2 in their chemosensory microvilli [8,12,13]. All three antisera specifically stained the sensory surface of the VNO. ANO2$_{in}$ immunostaining, but not ANO1 staining, was absent in sections from Ano2$^{-/-}$ mice. Preadsorption with the peptide that was used to raise ANO1$_{ex}$ suppressed the staining of ANO1 but not of ANO2. Cross reactivity of antisera against ANO1 and ANO2 was excluded by staining HEK 293 cells specifically transfected with either channel [33]. Rabbit anti-Cre antiserum (dilution 1:2000) [34] was kindly provided by Dr. Günther Schütz, DKFZ, Heidelberg. Secondary antibodies were goat anti-guinea pig with Alexa Fluor 488 (Molecular Probes A11073, dilution 1:1000) goat anti-guinea pig with Alexa Fluor 568 (Molecular Probes A11075, dilution 1:1000), goat anti-rabbit conjugated with Alexa Fluor 488 (Invitrogen A11008, dilution 1:1000), and goat anti-rabbit conjugated with Alexa Fluor 568 (Invitrogen A11011, dilution 1:1000).

Expression and molecular characterization of cerebellar Ano1 and Ano2

Semiquantitative RT-PCR analysis was performed on total RNA of cerebellum and, for comparison, on RNA from olfactory epithelium. RNA was isolated using the MagJet RNA Kit (Thermo Scientific). cDNA was synthesized using 5 µg total RNA, oligo (dT) 18 primer, and the Maxima H Minus First Strand cDNA Synthesis Kit (Thermo Scientific). PCR amplification

Table 1. PCR primer pairs used to characterize cerebellar ANO1 and ANO2.

Semiquantitative RT-PCR		
ANO1/F861	Forward	GGCCCGGTGACTACGTGTA
	Reverse	GCTGTGCCATTCTGGAAGTCGC
ANO2/F865	Forward	TTGAGATTGGAGTCCCGAAGCTAA
	Reverse	GGTGCCCATGGTGGTTCTCGATAA
Characterization of the splice variants		
ANO1/F851	Forward	ATGCAGGACGCGCAGGACA
	Reverse	GACTCCGTAACTTGCCCATTCC
ANO1/F855	Forward	CGCAGCGTCCACATCGTGAAC
	Reverse	ACTTGCCCATTCCTCATACAG
ANO1/F857	Forward	ATGAGGGTCCCCGAGAAGTACTC
	Reverse	CAGGAGGCCTCGCGTCTCA
ANO1/F847	Forward	CCCGGGAGAAGCAACACCTATT
	Reverse	AGTCACCGGGCCGACCAAC
ANO1/F845	Forward	CGGTGACTACGTGTACATCTTCC
	Reverse	GGCCTGTCATCATGGCTACAG
ANO2/F871	Forward	AGAGGAAGCCAGGGCCCCAAAC
	Reverse	CCGCTTCAGAATCTCGTGTAC
ANO2/F870	Forward	TGGGCTGCGAGACATCC
	Reverse	CCGCTTCAGAATCTCGTGTAC
ANO2/F869	Forward	CGCATGCACTTTCACGACAAC
	Reverse	CCGCTTCAGAATCTCGTGTAC
ANO2/F867	Forward	CCCCACCAAGAAAATGTACGAG
	Reverse	GGTAACCGTCGAACACGTAGACA
ANO2/R905	Forward	CCCTGACGTTCTCCATTGTC
	Reverse	CGGGCTCATACGTTGGTGTG
Full lenght cloning		
ANO1/F524	Forward	AGAATTCCACCATGAGGGTCCCCGAGAAGTACTC
	Reverse	TGGATCCAACAGCGCGTCCCCATGGTAC

doi:10.1371/journal.pone.0142160.t001

was performed on 1 μl (250 ng) single-stranded cDNA with DreamTaq PCR Master Mix (Thermo Scientific) using the primer pairs ANO1/F861 and ANO2/F865 (Table 1). Cycling conditions were 95°C for 3 min, followed by 28 to 34 cycles at, respectively, 95°C for 30 s, 62°C for 30 s, 72°C for 60 s, and finally 72°C for 8 min. The bands were resolved by gel electrophoresis and were verified by sequencing after purification by GeneJET Gel Extraction Kit (Thermo Scientific). To characterize the splice variants of the Ano1 and Ano2 transcripts, PCR was performed on cerebellar cDNA using the primers listed in Table 1. For Ano1, we used a set of 5 primer pairs which covered the entire transcript according to Genbank Acc. No. NM_178642.5. The forward primer of pair ANO1/F581 matched to the sequence at an alternative predicted translation start site (position 98 in NM_178642.5) and ANO1/F857 matched the sequence at the translation start site of isoform *a* (position 269). ANO1/F855, ANO1/F847 and ANO1/F845 consecutively matched the following sequence of the open reading frame. The primer pair ANO1/F581 resulted in no product while the four other primer pairs resulted in abundant PCR products of predicted size. By sequencing the PCR products, we found that the ANO1*ac* variant is expressed in the cerebellum. For ANO2, the primer pairs ANO2/F871, ANO2/F870 and ANO2/F869 consecutively matched the sequences of three alternative predicted translation start sites according to Genbank Acc. No. NM_153589.2. ANO2/F867, while

ANO2/F905 matched the remaining sequence of the open reading frame. PCR products of predicted size were obtained only for primer pairs ANO2/F869, ANO2/F867 and ANO2/F905, indicating that the first two alternative translation start sites are not present in the cerebellar transcript. By sequencing all PCR products, we found that the cerebellar ANO2 isoform is identical to the main olfactory isoform [6,9].

Immunoblot analysis

Main olfactory epithelium, eyes, olfactory bulb and cerebellar tissue were dissected from wild-type C57BL/6 (Black6) or Ano2$^{-/-}$ mice. A whole-protein extraction method was used for most of the samples. For biochemical assays of ANO2 expression in olfactory bulb and cerebellum, the Qproteome Cell Compartment Kit (Qiagen) was used for protein extraction because it was reported to produce particularly high yield of membrane protein [35]. The supernatant of fraction 2, containing primarily membrane proteins, was separated by SDS–PAGE on 10% gels and electro-blotted to PVDF membranes (Machery & Nagel; Germany) using a semidry blotting apparatus. Membranes were blocked with 5% milk powder (in PBS / 0.1% Tween 20) for 1 hour and incubated with the primary antibodies overnight. The blots were washed three times with 0.1% Tween 20 in PBS and incubated for 1 hour with a horseradish peroxidase-conjugated secondary antibody. The blots were washed again, and the *ECL plus* enhanced chemoluminescence system (GE Healthcare, Germany) was used to monitor bound antibodies. Antibodies used for immunoblotting were guinea-pig anti-ANO1 (dilution 1:400; C-terminus encoding amino acids 962–1040; marked "ANO1$_{in}$" in the text) [33], and a rabbit ANO2 antiserum directed against the extracellular loop that connects TMDs 5 and 6 in ANO2 (Alomone Labs, ACL012, dilution 1:1000, marked "ANO2$_{ex}$" in the text). The specificity of the ANO2$_{ex}$ antiserum was verified using olfactory epithelium and VNO, comparing wild-type and ANO2$^{-/-}$ mice. Furthermore, we used goat anti-actin (Santa Cruz sc-1615, dilution 1:1000), rabbit anti guinea pig HRP secondary antibody (Sigma, dilution 1:20000), goat anti rabbit HRP secondary antibody (Sigma, dilution 1:30000), donkey anti goat HRP secondary antibody (Jackson ImmunoResearch, dilution 1:10000).

EYFP-tagged Ano1 and Ano2 expression plasmids

For heterologous expression in HEK 293 cells, EYFP-tagged mouse cerebellar ANO1 and ANO2 were used. For ANO1*ac*, the primer pair ANO1/F524 (Table 1) was used for full length cloning from cerebellar cDNA. For controls, the ANO1*abc* isoform was amplified from mouse Ano1*abc* pCMV-SPORT6 plasmid (kindly provided by Dr. Rainer Schreiber und Dr. Karl Kunzelmann, University of Regensburg) using the same primers. An *EcoR*I site was introduced at the 5'end and a *BamH*I site at the 3' end of the fragments for fusing EYFP to the C-terminus in the expression vector pEYFP-N1 (Takara Bio Europe/Clontech, France). The ANO2-pEYFP-N1 expression plasmid was kindly provided by Dr. Johannes Reisert (Monell Chemical Senses Center, Philadelphia).

Electrophysiology

The cerebellum was removed from the skull directly after sacrificing the animals, and was mounted with cyanoacrylate glue in a vibratome chamber (Leica VT1000S) filled with the respective artificial cerebrospinal fluid (ACSF) at 34–37°C. Sagittal tissue slices were cut at 220–250 μm and transferred to an incubation chamber filled with ACSF at 34°C for 30 min. After this, the incubation chamber was kept at room temperature. All solutions were saturated with 95% O_2 / 5% CO_2 [36]. For patch-clamp experiments, we transferred the tissue slices onto the stage of an upright, water immersion microscope (Nikon Eclipse E600FN). The recording

chamber was continuously perfused with oxygenated ACSF at room temperature. Visual control was achieved with a camera system (Nikon DN100), and Purkinje cells were identified by their shape and location. To obtain whole-cell recordings, borosilicate glass micropipettes (Science Products, Hofheim, Germany; GB-150F-10) were made using a horizontal puller (Sutter Instruments; P97) to a resistance of 2–3 MΩ. Pipettes were filled with an intracellular solution and positioned on the Purkinje cell soma. After obtaining a tight seal, the plasma membrane inside the pipette tip was disrupted by suction to establish the whole-cell configuration. The drug perfusion system operated at 1–2 ml/min for a complete exchange of the bath solution. To block presynaptic cannabinoid receptors, which tend to reduce inhibitory signals [37], the CB1 antagonist *AM251* (2 µM) was included in the bath solution. Electrical signals were recorded using a patch-clamp amplifier (HEKA Electronics, Lambrecht, Germany; EPC-8) and the WinWCP (4.6.1) program provided by the University of Strathclyde, Glasgow, UK. Capacitance compensation was applied; series resistance was not compensated. Holding voltages were corrected for liquid junction potentials. Stimulation of climbing fibers was triggered by a constant current source (Digitimer, Welwyn Garden, UK; DS7A) through an ACSF-filled pipette. Postsynaptic currents were counted off-line before and after stimulation of climbing fibers. 3-minute traces were scanned by a peak-detection software (Mini-Analysis Program, Synaptosoft Inc.). Further analysis was performed using Igor Pro (WaveMetrics, version 6.34 A).

The following three intracellular solutions were used for Purkinje-cell electrophysiology: (1) for 131 mM $[Cl^-]_i$ (mM): 119 CsCl, 6 $MgCl_2$, 10 EGTA, 10 HEPES, 4 Na_2ATP, 19 sucrose; pH 7.3 with CsOH; (2) for 12 mM $[Cl^-]_i$ (mM): 119 Cs-methane sulfonate, 6 $MgCl_2$, 10 EGTA, 10 HEPES, 4 Na_2ATP, 19 sucrose; pH 7.3 with CsOH; (3) for 5 mM $[Cl^-]_i$ (mM): 150 Cs-methane sulfonate, 5 KCl, 0.1 Cs-EGTA, 10 Na-HEPES, 3 Mg-ATP, 0.4 Na-GTP; pH 7.4 with CsOH. ACSF for 131 mM $[Cl^-]_i$ experiments and 12 mM $[Cl^-]_i$ experiments (mM): 119 NaCl, 26.2 $NaHCO_3$, 2.5 KCl, 1 NaH_2PO_4, 1.3 $MgCl_2$, 2.5 $CaCl_2$, 33 glucose; pH 7.4 with HCl. ACSF for 5 mM $[Cl^-]_i$ experiments (mM): 138.6 NaCl, 21 $NaHCO_3$, 3.4 KCl, 0.6 NaH_2PO_4, 1 $MgCl_2$, 2.5 $CaCl_2$, 15 glucose; pH 7.4 with HCl. Drugs used were the ANO1-inhibitor *T16Ainh-A01* (Tocris Bioscience, 4538), the $GABA_A$ channel blocker picrotoxin (Sigma-Aldrich, P1675), and the cannabinoid receptor 1 antagonist *AM251* (Tocris Bioscience, 1117). Alexa Fluor 568 hydrazide sodium salt (Molecular Probes, A-10437, 50 µM) was used to visualize Purkinje cells.

For heterologous expression, EYFP-tagged mouse cerebellar Ano1 or Ano2 was transfected into HEK 293 cells by Ca^{2+}-phosphate co-precipitation. 24 h after transfection, expression was confirmed by yellow fluorescence, and cells were examined in whole-cell configuration at -70 mV. The bath solution contained (mM): 150 CsCl, 10 HEPES, 10 EGTA; pH 7.4 (CsOH); the pipette solutions contained 133.5 mM CsCl, 8.26 mM $CaCl_2$, 10 mM HEDTA, 10 mM HEPES; pH 7.0 (CsOH), to give a free Ca^{2+} concentration of 7.5 µM [38]. Currents were recorded immediately after whole-cell break-through as Ca^{2+} diffused into the cell. To evaluate the data for ANO2, the maximal current amplitudes were related to the individual cell capacitance. The current densities from 19–30 cells were averaged for each test. With ANO1 expressing cells, we did not obtain individual values for cell capacitance because large chloride conductances prevented accurate determination. In this case, current densities were calculated using the average cell capacitance of ANO2-expressing HEK 293 cells in our experiments. To test the effect of *T16Ainh-A01*, 5 µM of the compound were continuously included in the bath solution. Statistical analysis was done using Student´s *t* test. Error bars indicate SEM; significance levels were $p < 0.05$ (*), $p < 0.01$ (**), $p < 0.001$ (***) or $p < 0.0001$ (****).

Results

Detection of ANO1 and ANO2 expression in the mouse cerebellum

ANO1 and ANO2 channels are thought to have similar membrane topology. Hydropathy analyses and various functional assays have pointed to a model with 8 transmembrane domains [39–41] which was refined by X-ray crystallography to a 10 TMD model (Fig 1A) [42]. We compared the cerebellar expression levels of both genes with the olfactory neuroepithelium because the expression of both proteins is well characterized in that tissue [33]. The PCR signal for ANO1 cDNA was comparable between cerebellum and olfactory epithelium, while the ANO2 cDNA was weaker in cerebellum than in olfactory epithelium (Fig 1B). Both for ANO1 channels and for ANO2 channels, several alternative translation forms exist [5,6,41]. For ANO1, the positions of four relevant exons are indicated as a—d in Fig 1A. To identify the cerebellar ANO1 isoform, we used a set of 5 overlapping primer pairs (Table 1) that, together, covered the entire open reading frame of the transcript. By sequencing the PCR products, we found that the ANO1ac variant is expressed in the cerebellum. This isoform was previously shown to encode Cl$^-$ channels with particularly high apparent Ca^{2+} sensitivity ($K_D = 0.15$ μM at -40 mV; [5]). ANO2 proteins exist in the two isoforms A and B in olfactory receptor neurons [6] (Fig 1A). By sequencing the PCR products from cerebellum, we found the isoform B to be the predominant ANO2 variant. Isoform B is also the prevalent form in olfactory receptor neurons. It may contain a regulatory motif at a position homologous to segment c of ANO 1. This motif is present in photoreceptors but not in olfactory receptor neurons [26]. We found that it is also absent from the cerebellar ANO2 sequence. In immunoblots from membrane-protein preparations, the ANO1$_{in}$ serum labeled a band at the expected size of 115 kDa in olfactory
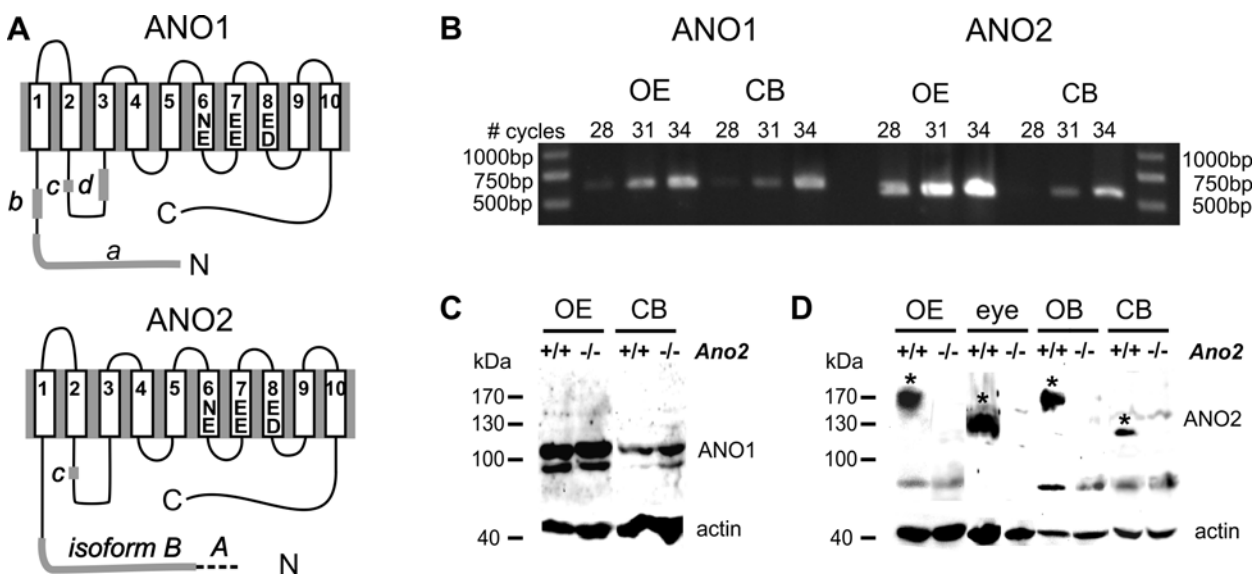

Fig 1. ANO1 and ANO2 expression levels in the cerebellum. (A) Membrane topology model for anoctamin Ca^{2+}-activated Cl$^-$ channels based on the X-ray structure of a fungal TMEM16 protein [42]. The transmembrane domains 5 and 6 are thought to provide the pore-lining region in the homodimeric channel [95]. Five negatively charged amino-acid residues *(E, D)* and an asparagine residue *(N)* in transmembrane domains 6–8 serve as Ca^{2+}-binding sites involved in channel gating [39–41]. Four alternatively spliced segments *(a—d)* determine the apparent Ca^{2+}-sensitivity of the ANO1 channel [5]. ANO2 has two isoforms *A* and *B* and a regulatory motif at a position homologous to segment *c* in ANO1 [6]. **(B)** RT-PCR analysis from mouse olfactory epithelium *(OE)* and mouse cerebellum *(CB)* yield similarly strong ANO1 signals in cerebellum but weaker signals for ANO2. **(C)** Immunoblots obtained from lysates of cerebellum *(CB)* and main olfactory epithelium *(OE)* from wild-type and Ano2$^{-/-}$ mice show an ANO1-specific signal at ~120 kDa with the ANO1$_{in}$ antiserum. **(D)** Rabbit anti-ANO2$_{ex}$ serum stains ANO2-specific bands *(asterisks)* in immunoblots obtained from lysates of main olfactory epithelium *(OE)* and eye, as well as in membrane-protein preparations of main olfactory bulb *(OB)* and cerebellum *(CB)*. ANO2 bands are not present in immunoblots from Ano2$^{-/-}$ mice.

epithelium and in cerebellum, both in wild-type and in Ano2$^{-/-}$ mice (Fig 1C). A weaker second band was visible at ~95 kDa. For detection of ANO2 protein, we used the ANO2$_{ex}$ antiserum which labeled a discrete band in cerebellum, as well as broader bands in preparations from olfactory epithelium, olfactory bulb and eye, all of which were absent in Ano2$^{-/-}$ mice (Fig 1D). These signals are characteristic for the glycosylated ANO2 protein at ~120 kDa in eye and at 150–170 kDa in olfactory tissues [8]. In our membrane-protein preparation, the cerebellar ANO2 protein appeared at ~120 kD with no evidence for pronounced glycosylation. These data consistently demonstrate that ANO1 and ANO2 proteins are expressed in the mouse cerebellum.

Differential expression of ANO1 and ANO2 in the cerebellar cortex

Purkinje cells, the large output neurons of the cerebellar cortex, receive excitatory input from granule cells and climbing fibers, as well as inhibitory input from stellate cells, basket cells and Golgi cells (Fig 2A). To find out which cells express ANO1 and ANO2, cryosections were prepared without pre-fixation of the tissue. DAB-labeled ANO1$_{in}$ antibodies stained the Purkinje cell layer as well as scattered cells in the molecular layer and granule cell layer (Fig 2B and 2C). Inhibitory interneurons in the granule cell layer (Fig 2D) and in the molecular layer (Fig 2E) were immunopositive both for ANO1 and for glutamate decarboxylase (GAD), a marker for GABAergic neurons. We used a mouse line that expressed Cre recombinase in all GAD67-expressing cells [32], and immunostained with an antiserum raised against Cre recombinase [34]. The labeled neurons in the granule cell layer are probably Golgi cells (Fig 2G) while the GAD/ANO1-positive cells in the molecular layer are basket/stellate cells (Fig 2H). Thus, apparently all GABAergic cells in the cerebellar cortex were ANO1-positive. The somata of Purkinje cells also expressed ANO1 (Fig 2F). Co-staining with the neuronal marker *NeuroTrace*® revealed that *all* Purkinje cells contained ANO1. However, ANO1 immunosignals were faint in, or absent from, the Purkinje cell dendrites. The preadsorption control with the immunizing peptide showed no immunosignal (Fig 2I).

Immunostaining of cerebellar cortex cryosections with ANO2$_{in}$ antiserum revealed a different expression pattern compared to ANO1. Like ANO1, the ANO2 immunosignal was absent from granule cells. However, ANO2 was also absent from the inhibitory interneurons. Instead, the protein was located in the Purkinje-cell dendrites (Fig 3A). Within the somata of Purkinje-cells, ANO2 immunosignals appeared to be confined to the perinuclear area, presumably the rough endoplasmic reticulum. This contrasts with ANO1 expression, as ANO1 protein can be detected all through the soma, but not in the dendrites (Fig 3B). For ANO2, a viable knockout mouse line is available [8]. To test the specificity of the cerebellar ANO2 signal, we stained cryosections of Ano2$^{-/-}$ mice and detected no immunosignals under the same experimental conditions (Fig 3C). The only other structure in the brain reported to be immunopositive for ANO2 is the olfactory bulb where the axons of olfactory receptor neurons coalesce onto glomeruli to form their synapses [8]. Fig 3D and Fig 3E depict the ANO2 immunosignal in olfactory bulb as a positive control and its absence from the Ano2$^{-/-}$ mouse.

These data reveal a differential expression pattern of ANO1 and ANO2 in the cerebellar cortex. Only ANO2 is present at detectable density in the dendrites, the site of synaptic plasticity of inhibitory transmission as discovered by Satoh et al. (2013) [31]. We, therefore, asked whether ANO2 may be involved in this process.

Plasticity of GABAergic inhibition is altered in Ano2$^{-/-}$ mice

Satoh et al. (2013) [31] found that Ca^{2+}-dependent Cl$^-$ currents were activated in Purkinje cells during stimulation of climbing fibers, and that these Cl$^-$ currents caused a depression of
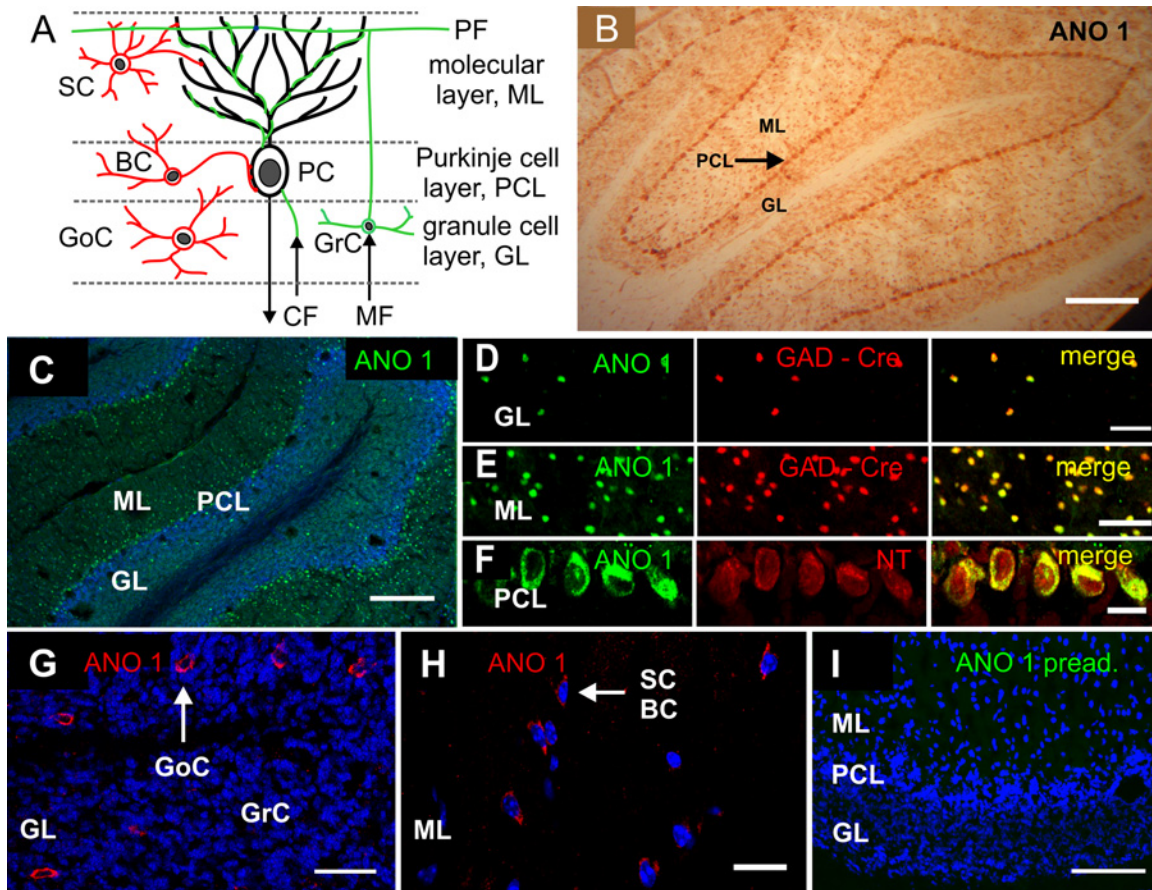
Fig 2. Expression of ANO1 in neurons of the cerebellar cortex. (A) Schematic representation of the main cell types that constitute the microcircuits of the cerebellar cortex. Inhibitory interneurons *(red)*: basket cells *(BC)*, Golgi cells *(GC)* and stellate cells (SC); excitatory input to Purkinje cells *(PC) (green)*: climbing fibers *(CF)*, granule cells *(GrC)*, mossy fibers *(MF)* and parallel fibers *(PF)*. **(B)** Diaminobenzidine-labelled $ANO1_{in}$ antiserum produced a continuous staining pattern in the Purkinje cell layer *(PCL)* as well as a scattered stain in the granule cell layer *(GL)* and the molecular layer *(ML)* of the mouse cerebellum. **(C)** Low-magnification image showing ANO1 immunofluorescence *(green)* and DAPI nuclear stain *(blue)*. Only few ANO1-positive cells are located among the many cells of the *GL*, most ANO-1 cells can be seen in the *PCL* and *ML*. **(D)** Detail of the *GL*, demonstrating co-localization of ANO1 and GAD^{Cre}, a marker for GABAergic neurons. **(E)** Co-localization of ANO1 with GAD^{Cre} cells in the *ML*. **(F)** Purkinje cell somata stained with the $ANO1_{ex}$ antiserum and *NeuroTrace*® to illustrate that all Purkinje cells are ANO1-positive. **(G)** Small, ANO1-negative granule-cell nuclei *(blue)* and somewhat larger ANO1-positive Golgi cells *(GoC)* in the *GL*. **(H)** In the molecular layer, ANO-1 positive cells are *SC* and *BC* inhibitory interneurons. **(I)** Preadsorption control for the $ANO1_{ex}$ antiserum on cerebellar cortex. Scale bars: *B, C*: 200 µm, *D,E*: 50 µm, *F*: 20 µm, *G*: 50 µm, *H*: 20 µm, *I*: 50 µM. Blue represents DAPI nuclear stain.

doi:10.1371/journal.pone.0142160.g002

GABAergic IPSCs recorded from Purkinje cells. To find out whether ANO2 is involved in this process, we compared the effect of climbing-fiber stimulation on IPSCs in wild type and $ANO2^{-/-}$ mice. Whole-cell recordings were obtained from sagittal tissue slices of mouse cerebellum. Purkinje cells located underneath the surface of the slice were identified by positions and shapes of their cell bodies and were selected for viability by their smooth, convex plasma membranes. A fluorescent dye was occasionally included in the pipette solution to visualize the dendritic tree ([Fig 4A]). Postsynaptic currents were recorded at a holding voltage V_{hold} of -69 mV and an intracellular Cl^- concentration $[Cl^-]_i$ of 131 mM. Detectable postsynaptic currents varied from a few pA to 819 pA (mean: 200.6 ± 5.8 pA). Their time course was characterized by a mean rise time (interval from 10% to 90% of maximal current) of 0.75 ± 0.007 ms, and a mean decay time constant (single-exponential fit) of τ = 5.54 ± 0.06 ms ([Fig 4B]; overlay of 764 signals). The signals were completely blocked by 50 µM picrotoxin in the bath solution ([Fig 4C]) and were thus pharmacologically identified as GABAergic currents. They originated from
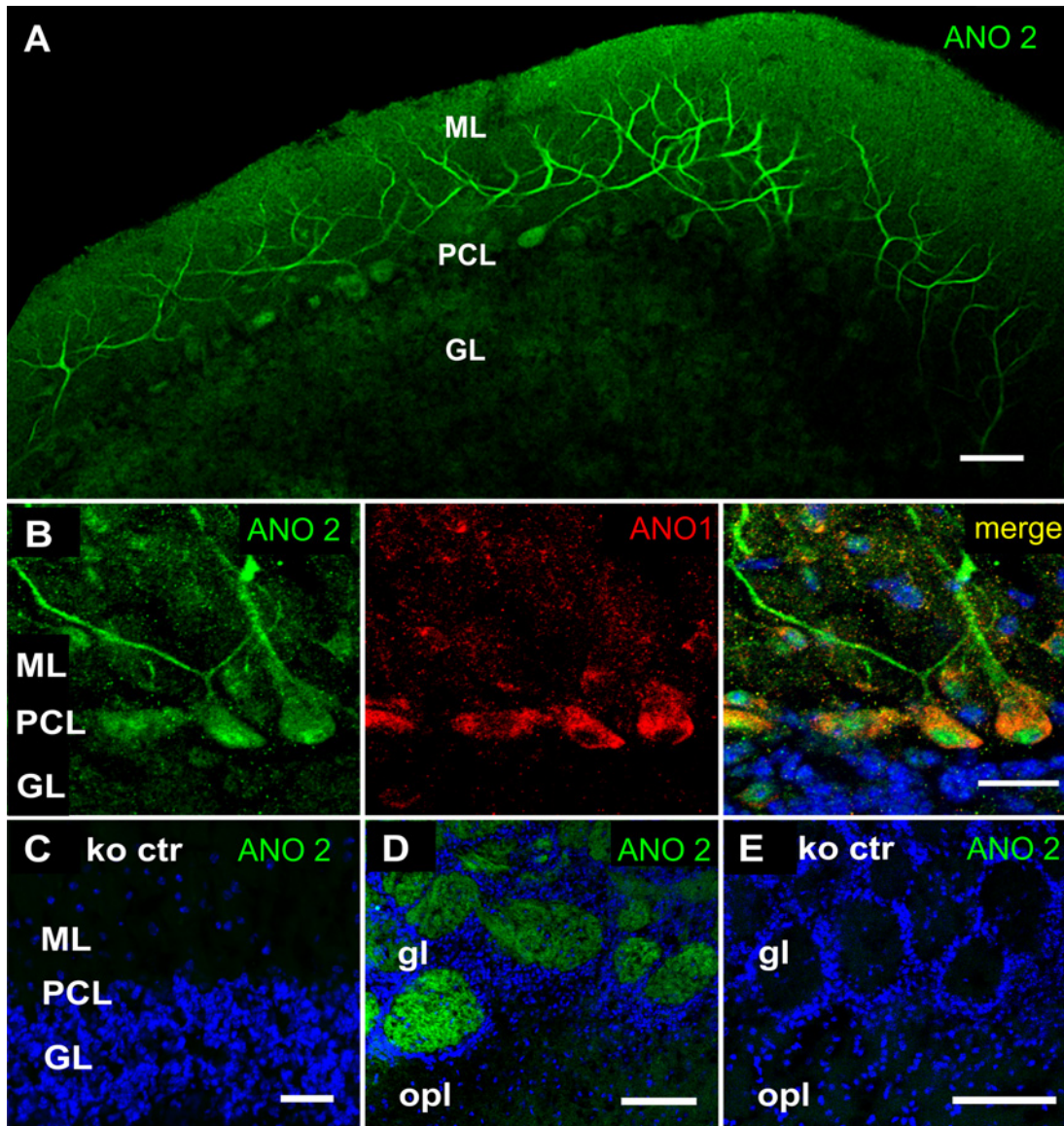
Fig 3. Expression of ANO2 protein in Purkinje cells. (A) ANO2 immunosignals from the cerebellar cortex are discernible in the dendrites of Purkinje cells. The signals are weak but stronger than the background signals emanating from the granule cell layer *(GL)*. **(B)** In the Purkinje cell, the ANO2 immunosignal *(green)* is visible in dendrites and the perinuclear region, but only weakly in the plasma membrane of the cell body. In contrast, ANO1 signals *(red)* label the entire Purkinje cell soma, but are not detectable in dendrites. **(C)** The ANO2 antiserum does not stain the cerebellar cortex of the Ano2$^{-/-}$ mouse. **(D)** ANO2 immunosignals in the glomeruli of the olfactory bulb serving as positive control for ANO2 in brain tissue; *gl*: glomerular layer, *opl*: outer plexiform layer. **(E)** Absence of ANO2 immunosignals from the olfactory bulb of the Ano2$^{-/-}$ mouse. Blue in *B-E* represents DAPI nuclear stain. All calibrations bars: 20 µm.

synapses that inhibitory interneurons (basket cells, stellate cells) form on the Purkinje cell dendrites and somata [43]. The negative polarity of these signals indicates that GABA$_A$ receptors conduct Cl$^-$ efflux at the high intracellular chloride concentration used. In these experiments, differences in amplitude may, in part, result from different local [Cl$^-$]$_i$ levels at each individual synapse. Moreover, electrical signals caused by dendritic postsynaptic currents in Purkinje cells are considerably attenuated and filtered as they travel along the dendrite toward the soma. With increasing distance between soma and the synaptic location on the dendritic tree, signal amplitudes decrease and time constants increase [44].
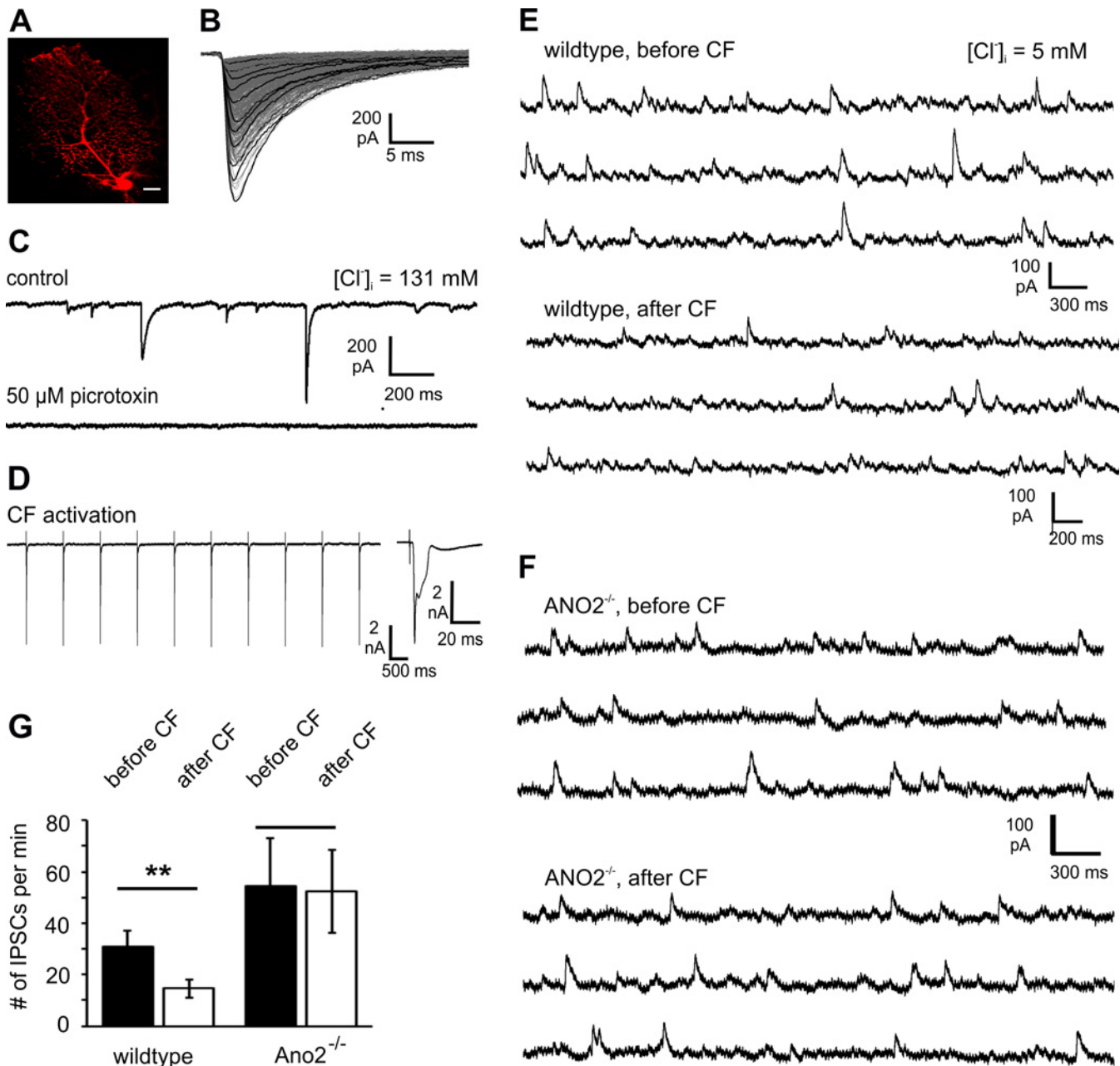
Fig 4. Involvement of ANO2 in depolarization-induced depression of inhibition. (A) A cerebellar Purkinje cell loaded with the fluorescent dye Alexa Fluor 568. Scale bar: 10 µm. (B) Spontaneous postsynaptic currents in a Purkinje cell with E_{Cl} near 0 mV and V_{hold} = -69 mV. Overlay of 764 current traces showing similar time courses but differing amplitudes, probably reflecting distinct positions of GABAergic synapses on the Purkinje cell dendritic tree. (C) Postsynaptic currents were completely blocked by 50 µM picrotoxin, an inhibitor of GABA$_A$-receptor chloride channels. (D) Protocol for activation of climbing fibers: Ten 0.1-ms current pulses were applied to the area near the proximal dendrite of a Purkinje cell while recording the whole-cell current of that cell at -70 mV. CF-activation produced characteristic complex spikes, as shown in the inset. (E) *Upper traces*: GABAergic inhibitory postsynaptic currents recorded from a Purkinje cell at V_{hold} = -48 mV and with 5 mM Cl$^-$ in the pipette solution. The positive polarity of IPSCs indicates Cl$^-$ influx. *Lower traces*: postsynaptic currents, recorded immediately after the climbing-fiber stimulation, displayed decreased amplitudes. (F) IPSCs recorded from a Purkinje cell of an Ano2$^{-/-}$ mouse before *(upper traces)* and immediately after *(lower traces)* CF-activation. (G) The number of detectable IPSC signals decreased by ~47% through climbing-fiber stimulation (before CF: 30.7 ± 6.5 min^{-1}; after CF: 14.6 ± 3.4 min^{-1}; 8 cells; *ctrl*). In slices from Ano2$^{-/-}$ mice, more IPSCs were detected (54.5 ± 18.5 min^{-1}; 4 cells), and the activation of climbing fibers had no effect (52.5 ± 16.2 min^{-1}; 4 cells).

ANO2 channels require more than 1 μM Ca^{2+} for full activation [9,11,38]. Dendritic Ca^{2+} influx was generated through synaptic activity of climbing fibers (CF) [45–47], which was triggered near the proximal dendrites of Purkinje cells through a stimulation pipette. CF activation designed to produce *DDI* (20 pulses at 1 Hz; Fig 4D) was confirmed by recording from the Purkinje cell the characteristic, prolonged Ca^{2+} currents that underlie complex-spike formation [48]. $[Cl^-]_i$ was set at 5 mM in these experiments (E_{Cl} = -88 mV) to obtain inhibitory postsynaptic currents from the GABAergic synapses. At V_{hold} between -60 mV and -45 mV, the synaptic signals were positive, indicative of postsynaptic Cl^- influx under this low-chloride condition (Fig 4E, *upper panel*). Following climbing-fiber stimulation, the recordings contained IPSC signal with reduced amplitudes (Fig 4E, *lower panel*). According to the concept of *DDI* [31], we interpret this reduced amplitude as indicative of a reduced Cl^- driving force for GABA-induced currents (see Discussion). To quantify the effect, we counted all IPSCs that were detected over 3 minutes. In ANO2$^{+/+}$ mice, the number of these signals decreased by 47% (8 cells) following climbing fiber stimulation (Fig 4G). The same experiments were carried out with cerebellar slices from ANO2$^{-/-}$ mice and revealed two differences compared to the wildtype: The number of IPSCs per minute before climbing-fiber activation was almost 2-fold higher, and it was not affected by climbing-fiber activation (Fig 4G). This observation is a strong indication for a role of ANO2 in the Ca^{2+}-dependent depression of inhibition described by Satoh et al. (2013) [31].

An ANO2 channel inhibitor mimics the effect of the ANO2 knockout

A reversible ANO2 channel inhibitor would be helpful to further investigate the physiological function of ANO2 in Purkinje cells. The widely used ANO1/ANO2 blocker niflumic acid was not suitable for our experiments because it is not specific for ANO2, and it is also known to have a potentiating effect on GABA$_A$ receptors [49]. The channel inhibitor *T16Ainh-A01* was originally identified as an ANO1 inhibitor in a small-molecule screen [50] and characterized in various cell types [50–52]. The efficacy of this compound in blocking anoctamin channels depends on the animal species and on the splice variant of the channels. In particular, *T16Ainh-A01* does not effectively inhibit mouse ANO1 [52], but strongly inhibits ANO2 channels [50]. To test its suitability for our experiments on cerebellar ANO2 channels, we expressed the cerebellar variants of murine ANO1 and ANO2 in HEK293 cells and examined their sensitivity to blockage by *T16Ainh-A01*. Transfected HEK 293 cells were perfused with pipette solution containing 7.5 μM Ca^{2+}, and the resulting currents were recorded at -70 mV immediately after whole-cell breakthrough (Fig 5A). This whole-cell method of channel blockage was used because it avoids channel alterations due to run-down, which ANO1 and ANO2 exhibit upon excision from the cell [26]. The average current densities were determined without inhibitor and compared to the values obtained in the presence of 5 μM or 25 μM *T16Ainh-A01*. In accordance with the report by Namkung et al. (2011) [50], the compound displayed a clear selectivity for ANO2 over ANO1 (Fig 5B). The compound did not affect currents conducted by mouse ANO1 channels at 5 μM, neither in the *abc* nor in the *ac* splice variant. Only at 25 μM *T16Ainh-A01* were ANO1*ac* channels significantly inhibited. In contrast, ANO2-mediated currents were reduced by 27% at 5 μM and by 60% at 25 μM. As 5 μM *T16Ainh-A01* selectively inhibits cerebellar ANO2 channels, we used this concentration to isolate pharmacologically any contribution of these channels to Purkinje cell activity. Although 5 μM *T16Ainh-A01* exerts only a moderate inhibitory effect on ANO2, it is suitable to experimentally distinguish ANO2 effects from any contributions by ANO1. In cerebellum slices incubated in ACSF containing 5 μM of the inhibitor, we recorded significantly increased IPSC numbers per minute. This elevated IPSC frequency was resistant to stimulation of climbing fibers (Fig 5C and 5D).
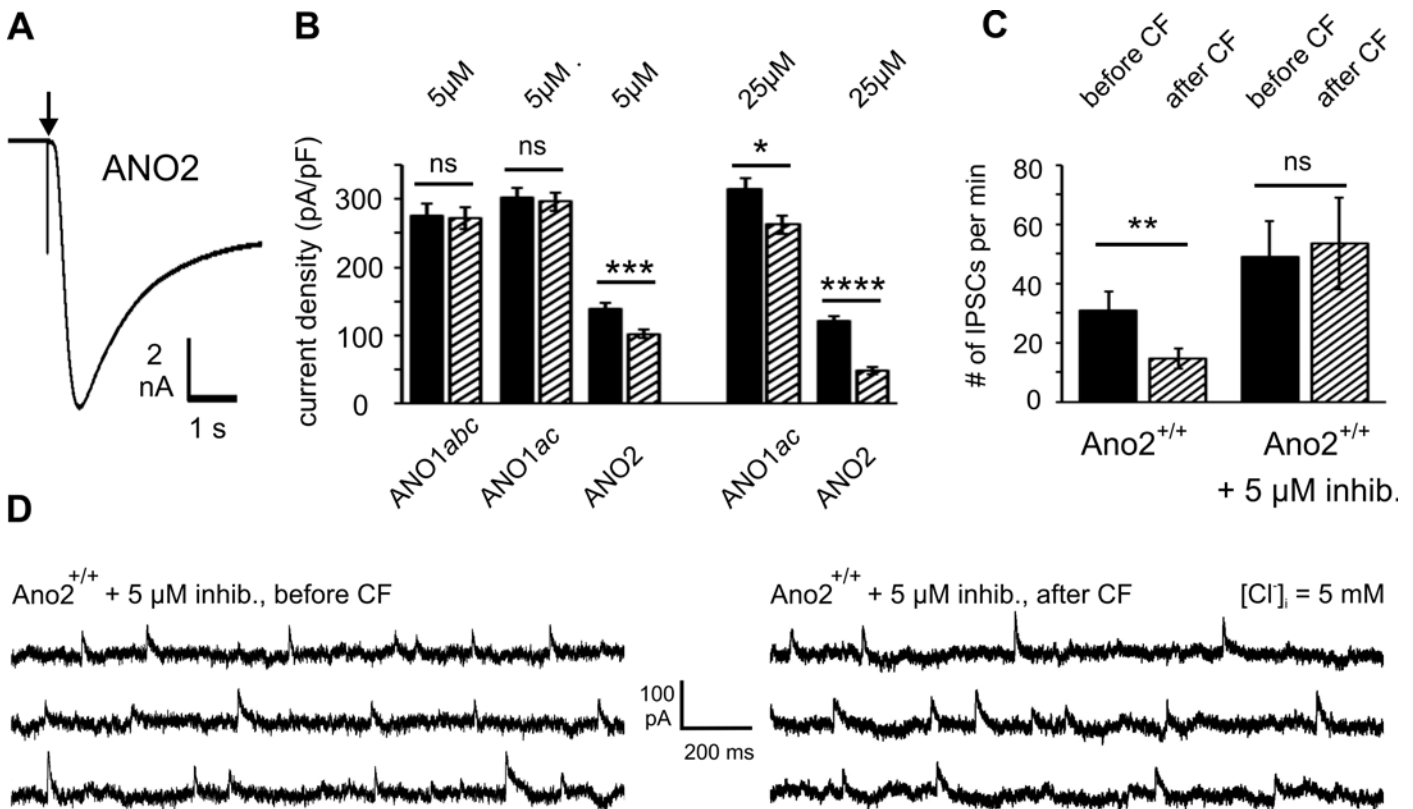
Fig 5. Identification of an inhibitor specific for cerebellar ANO2 channels. (A) Whole-cell recording from an HEK293 cell transfected with mouse cerebellar ANO2 isoform *B* at -70 mV. Chloride inward current was activated by diffusion of 7.5 μM Ca^{2+} from the pipette into the cell immediately after whole-cell breakthrough *(arrow)*. **(B)** Results from current recordings without *(black bars)* and with *(hatched bars)* T16Ainh-A01 revealed that neither mouse ANO1*ac* nor ANO1*abc* were significantly inhibited by 5 μM of the compound, while the ANO2 isoform *B* showed a significantly reduced current density. At 25 μM T16Ainh-A01, significant inhibition was also observed with ANO1*ac*. Results were averaged from 19–30 cells for each condition. **(C)** When applied at the ANO2-specific concentration of 5 μM, T16Ainh-A01 blocked *DDI*: The number of detectable IPSCs was 48.9 ± 12.1 min^{-1} before and 53.4 ± 15.4 min^{-1} after CF stimulation. ANO2$^{+/+}$ control data from [Fig 4G](#) are included for comparison. **(D)** IPSC traces from wildtype mice in the presence of 5 μM T16Ainh-A01 show no difference in IPSC shapes and amplitudes before *(left traces)* and after *(right traces)* CF-activation.

doi:10.1371/journal.pone.0142160.g005

In fact, the IPSC activities before and after the induction of complex spikes did not differ significantly between Ano2$^{-/-}$ mice and wild-type mice recorded with 5 μM channel inhibitor. These results further support the hypothesis that ANO2 mediates the plasticity of GABAergic inhibition in Purkinje cells.

Ionic plasticity may underlie the ANO2 effect on GABAergic inhibition

If ANO2 modulates IPSCs in GABAergic synapses by changing postsynaptic $[Cl^-]_i$, as suggested by the findings of Satoh et al. (2013) [31], the polarity and amplitude of IPSCs should depend on the activity of ANO2. We tested this assumption under conditions where a *reversal* of IPSC polarity may report an increase of $[Cl^-]_i$ at synaptic sites. We used 12 mM $[Cl^-]_i$ (E_{Cl} near -62 mV) in the pipette solution and clamped the holding-voltage to -60 mV. The rationale was to record GABAergic signals with E_{Cl} set close to V_{hold}, so that any driving force for Cl^- could only result from local changes of $[Cl^-]_i$ near the GABAergic synapses. Under these conditions, the postsynaptic currents had negative polarity indicating that E_{Cl} at the synaptic sites was more positive than V_{hold} and that $GABA_A$ receptors conducted Cl^- efflux ([Fig 6A](#)). Current amplitudes were small as a consequence of the small driving force for chloride ions
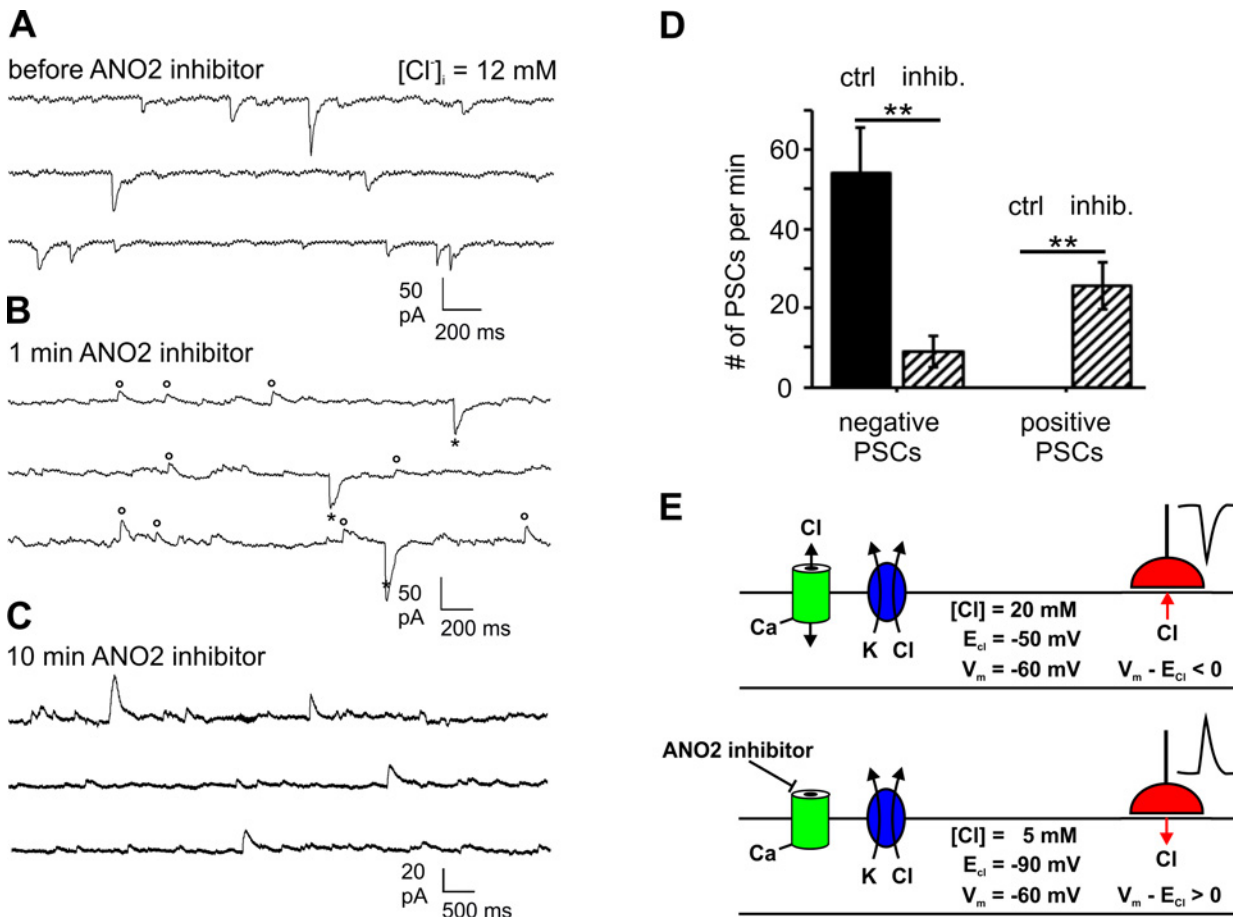
Fig 6. Reversal of GABAergic postsynaptic currents by the ANO2 inhibitor. (A) At a Cl$^-$ concentration of 12 mM in the recording pipette, GABAergic postsynaptic currents were negative (Cl$^-$ efflux), indicating that postsynaptic E_{Cl} is less negative than V_{hold}. **(B)** Shortly after applying 5 μM ANO2 inhibitor, positive currents appear *(circles)* as some synapses experience a decline of postsynaptic [Cl$^-$]$_i$, while others still have high Cl$^-$ *(asterisks)*. **(C)** During the continued presence of the ANO2 inhibitor, virtually all postsynaptic currents reverse to positive polarity (Cl$^-$ influx) indicating that GABAergic synapses experience an E_{Cl} more negative than V_{hold}. **(D)** The collected data from 12 Purkinje cells at [Cl$^-$]$_i$ = 12 mM and V_{hold} = -60 mV demonstrate the polarity reversal of postsynaptic currents (PSCs) actuated by the ANO2 inhibitor. **(E)** Schematic representation of an hypothesis for the 12 mM [Cl$^-$]$_i$ experiment. In the absence of the ANO2 inhibitor *(upper scheme)*, the basal activity of ANO2 channels *(green)* provides a Cl$^-$ conductance in the dendritic membrane. ANO2 contributes to the Cl$^-$ transport machinery, whose various pathways are represented by the K$^+$/Cl$^-$ cotransporter KCC2 *(blue)*. Together the Cl$^-$ pathways stabilize a slightly elevated level of [Cl$^-$]$_i$ which results in a negative driving force (V_m—E_{Cl} < 0) for Cl$^-$ currents through GABA$_A$ receptors in GABAergic synapses *(red)*. In this situation, Cl$^-$ currents are outwardly directed and cause negative postsynaptic currents. Application of the ANO2 inhibitor *(lower scheme)* reduces the Cl$^-$ conductance. This causes a polarity reversal of the Cl$^-$ driving force, as the balance shifts towards Cl$^-$ extrusion, causing local [Cl$^-$]$_i$ to decrease. This hypothesis provides a qualitative concept for the role of ANO2 channels in the inversion of postsynaptic currents that is depicted in panels A to C. The proximity of Cl$^-$ transport pathways and GABAergic synapses, as well as the occurrence of local Cl$^-$ gradients within dendritic segments, are inspired by the model for GABA$_A$-receptor-mediated Cl$^-$ gradients in extended dendritic trees proposed by Jedlicka et al. (2011) [88].

doi:10.1371/journal.pone.0142160.g006

(V_m—E_{Cl} < 0). Shortly after perfusion of the ANO2 inhibitor, both positive and negative signals were recorded ([Fig 6B](#)) and, upon continuous application of the inhibitor, most postsynaptic signals were inverted to positive polarity ([Fig 6C](#)). This effect of the inhibitor was observed at various times after the start of the experiment, but the polarity switch was never observed without the inhibitor. An analysis of signal traces from 9 Purkinje cells at 12 mM [Cl$^-$]$_i$ showed that the ANO2 inhibitor decreased the incidence of negative postsynaptic signals from 54.0 ± 11.6 min^{-1} to 9.0 ± 4.2 min^{-1}, while the incidence of positive signals increased from zero to 25.7 ± 6.0 min^{-1} ([Fig 6D](#)). Thus, application of the ANO2 inhibitor triggered a shift of the local E_{Cl} from a value more positive than V_{hold} to a value more negative than V_{hold}, caused by a

drop of local $[Cl^-]_i$ at the synaptic sites. This result is consistent with a modulatory effect of ANO2 on local $[Cl^-]_i$ under these conditions.

It appears that, at 12 mM $[Cl^-]_i$ in the pipette solution, the various chloride pathways present in the Purkinje cell dendrite uphold a chloride level that supports Cl^- efflux through $GABA_A$ receptors (Fig 6E, *upper scheme*). If, however, the ANO2 Cl^- conductance is blocked by *T16Ainh-A01* over a prolonged period of time, the balance between Cl^- uptake and Cl^- extrusion seems to change. Local $[Cl^-]_i$ decreases and promotes Cl^- influx through $GABA_A$ receptors (Fig 6E, *lower scheme*). This interpretation of the data presented in Fig 6 suggests that, even without experimentally induced climbing-fiber activation, ANO2 channels have a sufficient basal activity to influence local $[Cl^-]_i$ homeostasis near the synaptic sites. This may be the consequence of some excitatory input, and hence Ca^{2+} influx, in the slice preparation. These experiments suggest that ANO2 channels are a component of the transport system that regulates postsynaptic $[Cl^-]_i$ in the Purkinje-cell dendritic tree. As a Ca^{2+}-gated channel, ANO2 is expected to exert its effect most efficiently near sites of Ca^{2+} entry. We assume that the dendritic spines are the main source of Ca^{2+} entry [53], and that Ca^{2+} signals are strongest in the distal dendrites. This may be due to the larger surface-to-volume ratio and a higher density of voltage-gated Ca^{2+} channels in distal dendrites [54]. ANO2 in this region may contribute to *DDI* more efficiently than in the soma and proximal dendrite (see Discussion).

Taken together, the effects of the ANO2 inhibitor consistently demonstrate that ANO2 channels operate in the Purkinje cell plasma membrane. ANO2 appears to affect the regulation of local $[Cl^-]_i$ levels in the Purkinje cell dendritic tree. Under physiological low chloride conditions, ANO2 channels mediate a Ca^{2+}-dependent Cl^- uptake into the dendrite which causes an increase of local $[Cl^-]_i$ and, hence, a reduced driving force for Cl^- entry through $GABA_A$ channels. Thus, ANO2 channels appear to mediate depolarization-induced depression of inhibitory transmission, *DDI*, as described by Satoh et al. (2013) [31].

Discussion

ANO1 and ANO2 are expressed in the cerebellar cortex

We have examined the questions whether ANO1 and ANO2 proteins form Ca^{2+}-activated Cl^- channels in the cerebellar cortex, and whether these channels contribute to the *DDI* form of synaptic plasticity. PCR experiments and immunoblots showed that both ANO1 and ANO2 are expressed. Immunosignals indicated expression of both proteins in Purkinje cells, but ANO1 also in basket, stellate and Golgi cells. We identified the splice variant ANO1*ac*, a variant previously shown to possess particularly high Ca^{2+} sensitivity. The EC_{50} for channel activation by Ca^{2+} at -40 mV was reported to be 0.13 µM for ANO1*ac* and 0.63 µM for ANO1*abc* [5]. Segment *a* sensitizes ANO1 to Ca^{2+} [55], and segment *c* stabilizes the open state of the channel [56]. Immunostaining of ANO1 and ANO2 in the cerebellum required the preparation of cryosections without prefixation of the brain, a protocol known to increase detection sensitivity. Total protein extracts from tissue lysates did not produce anoctamin-specific signals in immunoblots, as reported earlier for ANO2 [8]. It was necessary to remove nuclei and soluble proteins and to enrich membrane proteins. These observations point to a relatively low expression level of ANO2 in the cerebellum, consistent with our RT-PCR analysis and immunostaining. The ANO1*ac* protein is expressed in all GABAergic neurons of the cerebellar cortex. Its function in these cells remains to be elucidated in future studies. In Purkinje cells, ANO1 appears to be restricted to the cell body and is hardly detectable in the dendritic tree. Possibly, the channels provide a Ca^{2+}-dependent component to cell volume control, as was suggested for ANO1 in epithelial cells [57]. It is, however, unlikely that ANO1*ac* channels contribute significantly to *DDI*. Because the application of 5 µM ANO2 inhibitor, as well as the ablation of the

Ano2 gene, completely removed *DDI*, our data strongly suggest that ANO2 channels mediate *DDI*.

The evidence for an involvement of ANO2 in ionic plasticity presented here is based on the comparison between wild-type Ano2$^{+/+}$ mice and Ano2$^{-/-}$ knockout mice. The availability of the Ano2$^{-/-}$ mouse line [8] strengthens the validity of the data, which would otherwise have to rely on the specificity of ANO2 antisera and the ANO2 inhibitor. However, the lack of dendritic ANO2 immunosignals in Ano2$^{-/-}$ Purkinje cells, together with the resistance of IPSCs to CF-stimulation in the knockout, strongly corroborate the hypothesis that ANO2 is necessary to trigger *DDI*. Nevertheless, it appears striking that the impact of 5 μM ANO2 inhibitor on IPSCs is strong enough to mimic the effect of an ANO2 knockout, considering that the blocker reduces ANO2 currents in HEK293 cells by only 27% at that concentration. This observation can be interpreted as a cumulative effect that developed during the extended presence of the blocker. The ANO2 inhibitor was applied for several minutes in our experiments. The continuously reduced dendritic Cl$^-$ permeability during this time is expected to result in a progressive change of dendritic [Cl$^-$]$_i$. Thus, temporal aspects have to be considered for the evaluation of the ANO2 inhibitor data. This is illustrated by Fig 6 where the inversion of postsynaptic current polarity is seen to develop with time.

Our data indicate that ANO2 channels are active even without climbing fiber activation and despite the presence of EGTA in our pipette solution. This is surprising, considering that Purkinje cells have a particularly high Ca^{2+} buffer capacity [58] and that the baseline Ca^{2+} concentration is expected to be low [47,59]. It indicates that, in our preparation, local Ca^{2+} fluctuations in the dendrites are sufficient to induce some degree of ANO2 activity. The isoform *B* of ANO2, which is expressed in Purkinje cells, is half-maximally activated at 1.33 μM Ca^{2+} [6]. Thus, channel activity, detected through effects of the channel blocker in the present study, may reflect Ca^{2+} concentrations of ~1 μM at the expression sites of ANO2. This points to a proximity of ANO2 channels and the sites of synaptic Ca^{2+}-signal generation in Purkinje-cell, the dendritic spines. It appears that the dendritic ANO2 channels respond to the Ca^{2+} concentration in the spines, and that they influence the local Cl$^-$ concentration inside the spines. The range of Ca^{2+}-concentrations in which cerebellar ANO2 channels operate (1–10 μM) [9,11,38] corresponds well to the dynamic range of Ca^{2+} transients measured in Purkinje cells. Ca^{2+} concentrations of 0.5 to 4 μM induce long-term depression upon activation of climbing fibers [59]. These matching Ca^{2+} ranges suggest that the open probability of dendritic ANO2 channels increases when excitatory synaptic inputs generate dendritic calcium signals through activation of voltage-gated Ca^{2+} channels and Ca^{2+} release (reviewed by [54]). ANO2 appears to be a Ca^{2+}-dependent element of chloride homeostasis in Purkinje cell dendritic spines. In concert with the chloride exporter KCC2 [60,61], the channels appear to set local levels of [Cl$^-$]$_i$ and, hence, to co-determine the efficacy of GABAergic transmission. A contribution of the chloride importer NKCC1 was suggested [31] because 50 μM bumetanide reduced an initial, transient phase of *DDI* that was observed in that study. However, expression of NKCC1 in Purkinje cells is not established; several studies report the absence of NKCC1 mRNA from Purkinje cells in the adult cerebellum [62–64].

ANO2 channels and synaptic plasticity in the cerebellum

The formation of procedural memory, in particular the acquisition of motor skills, involves the cerebellum as central element in the preparation, the execution, the fine adjustment, and in the learning of movement. The characteristically uniform microcircuits in the cerebellar cortex and the deep nuclei constitute the hub of signal processing for these tasks [65–68]. It is well documented that plasticity of inhibition in GABAergic synapses is a major factor in shaping

the output pattern of the cerebellar cortex [69–71]. The sites of plasticity are the synapses formed by inhibitory interneurons on the Purkinje cell dendrites and somata. Various distinct modes of synaptic plasticity control the efficacy of inhibitory transmission in these synapses: *rebound potentiation (RP)*, a postsynaptic Ca^{2+}/ CaMKII-mediated process that transiently enhances the responsiveness of $GABA_A$ receptors upon depolarization [72–75]; *depolarisation-induced potentiation of inhibition (DPI)*, a delayed, long-lasting increase of GABAergic transmission mediated by presynaptic NMDA-receptors [76]; *depolarization-induced suppression of inhibition (DSI)*, a reduction of IPSPs for ~20 s induced by retrograde inhibition of GABAergic synapses through endocannabinoids [37,77–79]; *depolarization-induced depression of inhibition (DDI)*, a decrease of IPSC amplitudes as a consequence of increasing postsynaptic Cl^- concentration, mediated by dendritic Ca^{2+}-activated Cl^- channels and, possibly, Cl^- transporters [31]. Taken together, these modes of synaptic plasticity reflect the relevance of modulatory processes for GABAergic inhibition of Purkinje cell activity.

The Ca^{2+}-dependent Cl^- conductance observed in Purkinje cells [77] was previously shown to be involved in the generation of *DDI* [31]. *DDI* changed the amplitudes of IPSCs that were evoked by stimulation of interneurons in the molecular layer and mediated by GABAergic synapses. The basic observation was that the postsynaptic currents transiently changed polarity from outward to inward (*i.e.* from inhibitory to excitatory), when a series of depolarizing pulses was applied to the Purkinje cells. Even after partial recovery and restoration of outward polarity, the IPSC amplitudes remained small for over 20 min. Satoh et al. (2013) [31] presented evidence that *DDI* was caused by a Ca^{2+}-dependent rise of $[Cl^-]_i$ on the postsynaptic side (in the Purkinje cell dendrite), resulting in a decreased driving force for Cl^- influx through $GABA_A$ receptors. As such, *DDI* would be an example of ionic plasticity [80–83], an altered synaptic transmission, brought about not by $GABA_A$ receptor regulation but because of a changing driving force for Cl^- flux.

In the present study, changes in $[Cl^-]_i$ were inferred from the effect of the ANO2 blocker on the amplitude of postsynaptic currents in GABAergic synapses. The interpretation of this indirect read-out is based on the assumption that the amplitudes of GABA-induced postsynaptic currents depend on $[Cl^-]_i$ and mirror any change of $[Cl^-]_i$. A decline of IPSC amplitude may, however, also be caused by changes in the neurotransmission process or by changes in the passive electrical properties of the dendrite. Such an electrical effect was proposed for ANO2 activation near excitatory synapses in hippocampal pyramidal neurons [27]. However, changes of GABA transmission in Purkinje cells following CF-activation occur on much slower time scales than used in this study [84] and require phosphorylation and recruitment of new receptor subunits. Moreover, it is unlikely that the decrease of IPSC amplitudes after CF-activation results from passive electrical effects like the introduction of a shunt conductance. This can be inferred from the effects of CF-activation on EPSPs at parallel-fiber synapses on Purkinje-cell dendrites. Time course and amplitude of EPSPS are not altered by CF-activation, provided that retrograde inhibition is blocked by a cannabinoid-receptor antagonist [85]. Thus, within the context of *DDI*, it is reasonable to assume that decrease and inversion of IPSCs observed here result from changes in $[Cl^-]_i$. Nevertheless, it would be desirable to directly measure changes of $[Cl^-]_i$ by chloride imaging, a method that was successfully applied to Purkinje cell dendrites using two photon excitation of the fluorescent dye MQAE [86]. This is technically demanding but may be a suitable approach to assess the contribution of ANO2 channels to $[Cl^-]_i$ regulation quantitatively.

The neuronal chloride homeostasis is mediated to a large extent by cation-chloride cotransporters, in particular by KCC2 and, in some neurons, by NKCC1 [87]. Chloride channels can, however, transiently change $[Cl^-]_i$, especially within the restricted space of distal dendrites [88–90]. This was studied in detail for the dendrites of hippocampal pyramidal neurons, where, as a

consequence of intense of $GABA_A$ receptor activity, $[Cl^-]_i$ increases and depolarizes E_{Cl} [91–93]. This GABA-induced Cl^- uptake can overcome the intrinsic Cl^- extrusion mechanism in parts of the dendrite with high density of inhibitory synapses. It can change E_{Cl} locally, and can hence cause a spatially restricted attenuation—or even inversion—of GABA effects [81]. In a similar way, ANO2 channels may affect $[Cl^-]_i$ and attenuate GABAergic input in the Purkinje cell dendrite, when activated by Ca^{2+} near excitatory synapses. In contrast to the homeostatic regulation of $[Cl^-]_i$ by cation-chloride cotransporters, the effect of ion channels on dendritic E_{Cl} ceases after Cl^- channels close and Cl^- extrusion prevails. Satoh et al. [31] reported, that Purkinje cells largely recovered from *DDI* within 2–3 minutes, but that inhibition was still slightly attenuated 20 min after *DDI* induction. If ANO2 channels mediate *DDI*, this slow time course of recovery reflects three processes following the end of CF-activation: return of dendritic Ca^{2+} levels to sub-micromolar levels, closing of ANO2 channels, and Cl^- extrusion from the dendrite. Ca^{2+}-imaging studies during CF-activation indicated that the Ca^{2+} decline proceeds within less than a second [58], and the open probability of ANO2 follows changes in Ca^{2+} concentration within a fraction of a second [11]. This suggests that the recovery dynamics of *DDI* are determined by the net rate of Cl^- extrusion. This rate may be determined by Cl^- imaging in future studies.

In conclusion, we have analyzed the expression of ANO1 and ANO2 Ca^{2+}-activated Cl^- channels in the cerebellar cortex. While ANO1 is expressed in inhibitory interneurons and in the somata of Purkinje cells, ANO2 is absent from inhibitory interneurons but specifically targeted to the Purkinje cell dendritic tree. ANO2 channels have previously been studied in dendritic signal processing of olfactory receptor neurons [6–10] and hippocampal pyramidal neurons [27] as well as in the pre-synaptic terminals of rod photoreceptors [14,15,94]. Here we provide evidence that dendritic ANO2 channels co-determine local chloride concentrations near GABAergic synapses. ANO2 channels appear to mediate *DDI*, a Ca^{2+}-dependent form of ionic plasticity that attenuates GABAergic inhibition in cerebellar Purkinje cells.

Acknowledgments

Author Contributions

Conceived and designed the experiments: DP SF FM. Performed the experiments: WZ SS. Analyzed the data: WZ SS SF FM. Wrote the paper: SF FM.

References

1. Pedemonte N, Galietta LJ (2014) Structure and function of TMEM16 proteins (anoctamins). Physiol Rev 94: 419–459. doi: 10.1152/physrev.00039.2011 PMID: 24692353

2. Caputo A, Caci E, Ferrera L, Pedemonte N, Barsanti C, Sondo E, et al. (2008) TMEM16A, a membrane protein associated with calcium-dependent chloride channel activity. Science 322: 590–594. doi: 10.1126/science.1163518 PMID: 18772398

3. Schroeder BC, Cheng T, Jan YN, Jan LY (2008) Expression cloning of TMEM16A as a calcium-activated chloride channel subunit. Cell 134: 1019–1029. doi: 10.1016/j.cell.2008.09.003 PMID: 18805094

4. Yang YD, Cho HW, Koo JY, Tak MH, Cho Y, Shim WS, et al. (2008) TMEM16A confers receptor-activated calcium-dependent chloride conductance. Nature 455: 1210–1216. doi: 10.1038/nature07313 PMID: 18724360

5. Ferrera L, Caputo A, Ubby I, Bussani E, Zegarra-Moran O, Ravazzolo R, et al. (2009) Regulation of TMEM16A Chloride Channel Properties by Alternative Splicing. J Biol Chem 284: 33360–33368. doi: 10.1074/jbc.M109.046607 PMID: 19819874

6. Ponissery Saidu S, Stephan AB, Talaga AK, Zhao H, Reisert J (2013) Channel properties of the splicing isoforms of the olfactory calcium-activated chloride channel Anoctamin 2. J Gen Physiol 141: 691–703. doi: 10.1085/jgp.201210937 PMID: 23669718

7. Hengl T, Kaneko H, Dauner K, Vocke K, Frings S, Möhrlen F (2010) Molecular components of signal amplification in olfactory sensory cilia. Proc Natl Acad Sci U S A 107: 6052–6057. doi: 10.1073/pnas.0909032107 PMID: 20231443

8. Billig GM, Pal B, Fidzinski P, Jentsch TJ (2011) Ca2+-activated Cl- currents are dispensable for olfaction. Nat Neurosci 14: 763–769. doi: 10.1038/nn.2821 PMID: 21516098

9. Stephan AB, Shum EY, Hirsh S, Cygnar KD, Reisert J, Zhao H (2009) ANO2 is the cilial calcium-activated chloride channel that may mediate olfactory amplification. Proc Natl Acad Sci U S A 106: 11776–11781. doi: 10.1073/pnas.0903304106 PMID: 19561302

10. Rasche S, Toetter B, Adler J, Tschapek A, Doerner JF, Kurtenbach S, et al. (2010) Tmem16b is Specifically Expressed in the Cilia of Olfactory Sensory Neurons. Chem Senses 35: 239–245. doi: 10.1093/chemse/bjq007 PMID: 20100788

11. Pifferi S, Dibattista M, Menini A (2009) TMEM16B induces chloride currents activated by calcium in mammalian cells. Pflugers Archiv-Eur J Physiol 458: 1023–1038.

12. Dibattista M, Amjad A, Maurya DK, Sagheddu C, Montani G, Tirindelli R, et al. (2012) Calcium-activated chloride channels in the apical region of mouse vomeronasal sensory neurons. J Gen Physiol 140: 3–15. doi: 10.1085/jgp.201210780 PMID: 22732308

13. Amjad A, Hernandez-Clavijo A, Pifferi S, Maurya DK, Boccaccio A, Franzot J, et al. (2015) Conditional knockout of TMEM16A/anoctamin1 abolishes the calcium-activated chloride current in mouse vomeronasal sensory neurons. J Gen Physiol.

14. Stöhr H, Heisig JB, Benz PM, Schoberl S, Milenkovic VM, Strauss O, et al. (2009) TMEM16B, A Novel Protein with Calcium-Dependent Chloride Channel Activity, Associates with a Presynaptic Protein Complex in Photoreceptor Terminals. J Neurosci 29: 6809–6818. doi: 10.1523/JNEUROSCI.5546-08.2009 PMID: 19474308

15. Dauner K, Mobus C, Frings S, Möhrlen F (2013) Targeted expression of anoctamin calcium-activated chloride channels in rod photoreceptor terminals of the rodent retina. Invest Ophthalmol Vis Sci 54: 3126–3136. doi: 10.1167/iovs.13-11711 PMID: 23557741

16. Jeon JH, Paik SS, Chun MH, Oh U, Kim IB (2013) Presynaptic Localization and Possible Function of Calcium-Activated Chloride Channel Anoctamin 1 in the Mammalian Retina. PLoS One 8: e67989. PMID: 23840801

17. Jeon JH, Park JW, Lee JW, Jeong SW, Yeo SW, Kim IB (2011) Expression and immunohistochemical localization of TMEM16A/anoctamin 1, a calcium-activated chloride channel in the mouse cochlea. Cell Tissue Res 345: 223–230. doi: 10.1007/s00441-011-1206-6 PMID: 21779783

18. Cho SJ, Jeon JH, Chun do I, Yeo SW, Kim IB (2014) Anoctamin 1 expression in the mouse auditory brainstem. Cell Tissue Res 357: 563–569. doi: 10.1007/s00441-014-1897-6 PMID: 24853671

19. Zhang XD, Lee JH, Lv P, Chen WC, Kim HJ, Wei D, et al. (2015) Etiology of distinct membrane excitability in pre- and posthearing auditory neurons relies on activity of Cl- channel TMEM16A. Proc Natl Acad Sci U S A 112: 2575–2580. doi: 10.1073/pnas.1414741112 PMID: 25675481

20. Cho H, Yang YD, Lee J, Lee B, Kim T, Jang Y, et al. (2012) The calcium-activated chloride channel anoctamin 1 acts as a heat sensor in nociceptive neurons. Nat Neurosci 15: 1015–1021. doi: 10.1038/nn.3111 PMID: 22634729

21. Lee B, Cho H, Jung J, Yang YD, Yang DJ, Oh U (2014) Anoctamin 1 contributes to inflammatory and nerve-injury induced hypersensitivity. Mol Pain 10: 5. doi: 10.1186/1744-8069-10-5 PMID: 24450308

22. Garcia G, Martinez-Rojas VA, Rocha-Gonzalez HI, Granados-Soto V, Murbartian J (2014) Evidence for the participation of Ca(2+)-activated chloride channels in formalin-induced acute and chronic nociception. Brain Res 1579: 35–44. doi: 10.1016/j.brainres.2014.07.011 PMID: 25036442

23. Kanazawa T, Matsumoto S (2014) Expression of transient receptor potential vanilloid 1 and anoctamin 1 in rat trigeminal ganglion neurons innervating the tongue. Brain Res Bull 106: 17–20. doi: 10.1016/j.brainresbull.2014.04.015 PMID: 24792786

24. Jin X, Shah S, Liu Y, Zhang H, Lees M, Fu Z, et al. (2013) Activation of the Cl- channel ANO1 by localized calcium signals in nociceptive sensory neurons requires coupling with the IP3 receptor. Sci Signal 6: ra73. doi: 10.1126/scisignal.2004184 PMID: 23982204

25. Liu B, Linley JE, Du X, Zhang X, Ooi L, Zhang H, et al. (2010) The acute nociceptive signals induced by bradykinin in rat sensory neurons are mediated by inhibition of M-type K+ channels and activation of Ca2+-activated Cl- channels. J Clin Invest 120: 1240–1252. doi: 10.1172/JCI41084 PMID: 20335661

26. Vocke K, Dauner K, Hahn A, Ulbrich A, Broecker J, Keller S, et al. (2013) Calmodulin-dependent activation and inactivation of anoctamin calcium-gated chloride channels. J Gen Physiol 142: 381–404. doi: 10.1085/jgp.201311015 PMID: 24081981

27. Huang WC, Xiao S, Huang F, Harfe BD, Jan YN, Jan LY (2012) Calcium-activated chloride channels (CaCCs) regulate action potential and synaptic response in hippocampal neurons. Neuron 74: 179–192. doi: 10.1016/j.neuron.2012.01.033 PMID: 22500639

28. Takayama Y, Shibasaki K, Suzuki Y, Yamanaka A, Tominaga M (2014) Modulation of water efflux through functional interaction between TRPV4 and MEM16A/anoctamin 1. FASEB J 28: 2238–2248. doi: 10.1096/fj.13-243436 PMID: 24509911

29. Thomas-Gatewood C, Neeb ZP, Bulley S, Adebiyi A, Bannister JP, Leo MD, et al. (2011) TMEM16A channels generate Ca2+-activated Cl- currents in cerebral artery smooth muscle cells. Am J Physiol-Heart Circ Physiol 301: H1819–H1827. doi: 10.1152/ajpheart.00404.2011 PMID: 21856902

30. Bulley S, Neeb ZP, Burris SK, Bannister JP, Thomas-Gatewood CM, Jangsangthong W, et al. (2012) TMEM16A/ANO1 channels contribute to the myogenic response in cerebral arteries. Circ Res 111: 1027–1036. PMID: 22872152

31. Satoh H, Qu L, Suzuki H, Saitow F (2013) Depolarization-induced depression of inhibitory transmission in cerebellar Purkinje cells. Physiol Rep 1: e00061. doi: 10.1002/phy2.61 PMID: 24303140

32. Tolu S, Avale ME, Nakatani H, Pons S, Parnaudeau S, Tronche F, et al. (2010) A versatile system for the neuronal subtype specific expression of lentiviral vectors. FASEB J 24: 723–730. doi: 10.1096/fj.09-139790 PMID: 19858094

33. Dauner K, Lissmann J, Jeridi S, Frings S, Möhrlen F (2012) Expression patterns of anoctamin 1 and anoctamin 2 chloride channels in the mammalian nose. Cell Tissue Res 347: 327–341. doi: 10.1007/s00441-012-1324-9 PMID: 22314846

34. Kellendonk C, Tronche F, Casanova E, Anlag K, Opherk C, Schütz G (1999) Inducible site-specific recombination in the brain. J Mol Biol 285: 175–182. PMID: 9878397

35. Bunger S, Roblick UJ, Habermann JK (2009) Comparison of five commercial extraction kits for subsequent membrane protein profiling. Cytotechnol 61: 153–159.

36. Huang S, Uusisaari MY (2013) Physiological temperature during brain slicing enhances the quality of acute slice preparations. Front Cell Neurosci 7: 48. doi: 10.3389/fncel.2013.00048 PMID: 23630465

37. Diana MA, Levenes C, Mackie K, Marty A (2002) Short-term retrograde inhibition of GABAergic synaptic currents in rat Purkinje cells is mediated by endogenous cannabinoids. J Neurosci 22: 200–208. PMID: 11756503

38. Reisert J, Bauer PJ, Yau KW, Frings S (2003) The Ca-activated Cl channel and its control in rat olfactory receptor neurons. J Gen Physiol 122: 349–363. PMID: 12939394

39. Tien J, Peters CJ, Wong XM, Cheng T, Jan YN, Yan LY, et al. (2014) A comprehensive search for calcium binding sites critical for TMEM16A calcium-activated chloride channel activity. Elife: e02772.

40. Bill A, Popa MO, van Diepen MT, Gutierrez A, Lilley S, Velkova M, et al. (2015) Variomics screen identifies the reentrant loop of the calcium-activated chloride channel ANO1 that facilitates channel activation. J Biol Chem 290: 889–903. doi: 10.1074/jbc.M114.618140 PMID: 25425649

41. Yu K, Duran C, Qu Z, Cui YY, Hartzell HC (2012) Explaining calcium-dependent gating of anoctamin-1 chloride channels requires a revised topology. Circ Res 110: 990–999. doi: 10.1161/CIRCRESAHA.112.264440 PMID: 22394518

42. Brunner JD, Lim NK, Schenck S, Duerst A, Dutzler R (2014) X-ray structure of a calcium-activated TMEM16 lipid scramblase. Nature 516: 207–212. doi: 10.1038/nature13984 PMID: 25383531

43. Konnerth A, Llano I, Armstrong CM (1990) Synaptic currents in cerebellar Purkinje cells. Proc Natl Acad Sci U S A 87: 2662–2665. PMID: 2015639

44. Roth A, Hausser M (2001) Compartmental models of rat cerebellar Purkinje cells based on simultaneous somatic and dendritic patch-clamp recordings. J Physiol 535: 445–472. PMID: 11533136

45. Kitamura K, Hausser M (2011) Dendritic calcium signaling triggered by spontaneous and sensory-evoked climbing fiber input to cerebellar Purkinje cells in vivo. J Neurosci 31: 10847–10858. doi: 10.1523/JNEUROSCI.2525-10.2011 PMID: 21795537

46. Miyakawa H, Lev-Ram V, Lasser-Ross N, Ross WN (1992) Calcium transients evoked by climbing fiber and parallel fiber synaptic inputs in guinea pig cerebellar Purkinje neurons. J Neurophysiol 68: 1178–1189. PMID: 1359027

47. Konnerth A, Dreessen J, Augustine GJ (1992) Brief dendritic calcium signals initiate long-lasting synaptic depression in cerebellar Purkinje cells. Proc Natl Acad Sci U S A 89: 7051–7055. PMID: 1323125

48. Schmolesky MT, Weber JT, De Zeeuw CI, Hansel C (2002) The making of a complex spike: ionic composition and plasticity. Ann N Y Acad Sci 978: 359–390. PMID: 12582067

49. Sinkkonen ST, Mansikkamaki S, Moykkynen T, Luddens H, Uusi-Oukari M, Korpi ER (2003) Receptor subtype-dependent positive and negative modulation of GABA(A) receptor function by niflumic acid, a nonsteroidal anti-inflammatory drug. Mol Pharmacol 64: 753–763. PMID: 12920213

50. Namkung W, Phuan PW, Verkman AS (2011) TMEM16A Inhibitors Reveal TMEM16A as a Minor Component of Calcium-activated Chloride Channel Conductance in Airway and Intestinal Epithelial Cells. J Biol Chem 286: 2365–2374. doi: 10.1074/jbc.M110.175109 PMID: 21084298

51. Bradley E, Fedigan S, Webb T, Hollywood MA, Thornbury KD, McHale NG, et al. (2014) Pharmacological characterization of TMEM16A currents. Channels (Austin) 8: 308–320.

52. Liu Y, Zhang H, Huang D, Qi J, Xu J, Gamper N, et al. (2015) Characterization of the effects of Cl channel modulators on TMEM16A and bestrophin-1 Ca activated Cl channels. Pflugers Arch. 467: 1417–1430. doi: 10.1007/s00424-014-1572-5 PMID: 25078708

53. Hartmann J, Konnerth A (2005) Determinants of postsynaptic Ca2+ signaling in Purkinje neurons. Cell Calcium 37: 459–466. PMID: 15820394

54. Kitamura K, Kano M (2013) Dendritic calcium signaling in cerebellar Purkinje cell. Neural Netw 47: 11–17. doi: 10.1016/j.neunet.2012.08.001 PMID: 22985934

55. Yang T, Hendrickson WA, Colecraft HM (2014) Preassociated apocalmodulin mediates Ca2+-dependent sensitization of activation and inactivation of TMEM16A/16B Ca2+-gated Cl- channels. Proc Natl Acad Sci U S A 111: 18213–18218. doi: 10.1073/pnas.1420984111 PMID: 25489088

56. Xiao Q, Yu K, Perez-Cornejo P, Cui Y, Arreola J, Hartzell HC (2011) Voltage- and calcium-dependent gating of TMEM16A/ Ano1 chloride channels are physically coupled by the first intracellular loop. Proc Natl Acad Sci U S A 108: 8891–8896. doi: 10.1073/pnas.1102147108 PMID: 21555582

57. Almaca J, Tian Y, Aldehni F, Ousingsawat J, Kongsuphol P, Rock JR, et al. (2009) TMEM16 proteins produce volume-regulated chloride currents that are reduced in mice lacking TMEM16A. J Biol Chem 284: 28571–28578. doi: 10.1074/jbc.M109.010074 PMID: 19654323

58. Eilers J, Plant T, Konnerth A (1996) Localized calcium signalling and neuronal integration in cerebellar Purkinje neurones. Cell Calcium 20: 215–226. PMID: 8889210

59. Finch EA, Tanaka K, Augustine GJ (2012) Calcium as a trigger for cerebellar long-term synaptic depression. Cerebellum 11: 706–717. PMID: 21975855

60. Huang Y, Ko H, Cheung ZH, Yung KK, Yao T, Wang JJ, et al. (2012) Dual actions of brain-derived neurotrophic factor on GABAergic transmission in cerebellar Purkinje neurons. Exp Neurol 233: 791–798. doi: 10.1016/j.expneurol.2011.11.043 PMID: 22178325

61. Kawakita I, Uchigashima M, Konno K, Miyazaki T, Yamasaki M, Watanabe M (2013) Type 2 K+ -Cl-cotransporter is preferentially recruited to climbing fiber synapses during development and the stellate cell-targeting dendritic zone at adulthood in cerebellar Purkinje cells. Eur J Neurosci 37: 532–543. doi: 10.1111/ejn.12076 PMID: 23216656

62. Kanaka C, Ohno K, Okabe A, Kuriyama K, Itoh T, Fukuda A, et al. (2001) The differential expression patterns of messenger RNAs encoding K-Cl cotransporters (KCC1,2) and Na-K-2Cl cotransporter (NKCC1) in the rat nervous system. Neuroscience 104: 933–946. PMID: 11457581

63. Mikawa S, Wang C, Shu F, Wang T, Fukuda A, Sato K (2002) Developmental changes in KCC1, KCC2 and NKCC1 mRNAs in the rat cerebellum. Brain Res Dev Brain Res 136: 93–100. PMID: 12101026

64. Seja P, Schonewille M, Spitzmaul G, Badura A, Klein I, Rudhard Y, et al. (2012) Raising cytosolic Cl- in cerebellar granule cells affects their excitability and vestibulo-ocular learning. EMBO J 31: 1217–1230. doi: 10.1038/emboj.2011.488 PMID: 22252133

65. Marr D (1969) A theory of cerebellar cortex. J Physiol 202: 437–470. PMID: 5784296

66. Ito M (1970) Neurophysiological aspects of the cerebellar motor control system. Int J Neurol 7: 162–176. PMID: 5499516

67. Eccles JC (1967) Circuits in the cerebellar control of movement. Proc Natl Acad Sci U S A 58: 336–343. PMID: 5231614

68. Albus JS (1971) Theory of cerebellar function. Mathematical Biosciences 10: 25–61.

69. Duguid IC, Pankratov Y, Moss GW, Smart TG (2007) Somatodendritic release of glutamate regulates synaptic inhibition in cerebellar Purkinje cells via autocrine mGluR1 activation. J Neurosci 27: 12464–12474. PMID: 18003824

70. De Zeeuw CI, Hoebeek FE, Bosman LW, Schonewille M, Witter L, Koekkoek SK (2011) Spatiotemporal firing patterns in the cerebellum. Nat Rev Neurosci 12: 327–344. doi: 10.1038/nrn3011 PMID: 21544091

71. Kullmann DM, Moreau AW, Bakiri Y, Nicholson E (2012) Plasticity of inhibition. Neuron 75: 951–962. doi: 10.1016/j.neuron.2012.07.030 PMID: 22998865

72. Kano M, Fukunaga K, Konnerth A (1996) Ca(2+)-induced rebound potentiation of gamma-aminobutyric acid-mediated currents requires activation of Ca2+/calmodulin-dependent kinase II. Proc Natl Acad Sci U S A 93: 13351–13356. PMID: 8917594

73. Kano M, Rexhausen U, Dreessen J, Konnerth A (1992) Synaptic excitation produces a long-lasting rebound potentiation of inhibitory synaptic signals in cerebellar Purkinje cells. Nature 356: 601–604. PMID: 1313949

74. Kawaguchi SY, Hirano T (2002) Signaling cascade regulating long-term potentiation of GABA(A) receptor responsiveness in cerebellar Purkinje neurons. J Neurosci 22: 3969–3976. PMID: 12019316

75. Hashimoto T, Ishii T, Ohmori H (1996) Release of Ca2+ is the crucial step for the potentiation of IPSCs in the cultured cerebellar Purkinje cells of the rat. J Physiol 497: 611–627. PMID: 9003548

76. Duguid IC, Smart TG (2004) Retrograde activation of presynaptic NMDA receptors enhances GABA release at cerebellar interneuron-Purkinje cell synapses. Nat Neurosci 7: 525–533. PMID: 15097992

77. Llano I, Leresche N, Marty A (1991) Calcium entry increases the sensitivity of cerebellar Purkinje cells to applied GABA and decreases inhibitory synaptic currents. Neuron 6: 565–574. PMID: 2015092

78. Kreitzer AC, Regehr WG (2002) Retrograde signaling by endocannabinoids. Curr Op Neurobiol 12: 324–330. PMID: 12049940

79. Yoshida T, Hashimoto K, Zimmer A, Maejima T, Araishi K, Kano M (2002) The cannabinoid CB1 receptor mediates retrograde signals for depolarization-induced suppression of inhibition in cerebellar Purkinje cells. J Neurosci 22: 1690–1697. PMID: 11880498

80. Kaila K, Ruusuvuori E, Seja P, Voipio J, Puskarjov M (2014) GABA actions and ionic plasticity in epilepsy. Curr Opin Neurobiol 26: 34–41. doi: 10.1016/j.conb.2013.11.004 PMID: 24650502

81. Blaesse P, Airaksinen MS, Rivera C, Kaila K (2009) Cation-chloride cotransporters and neuronal function. Neuron 61: 820–838. doi: 10.1016/j.neuron.2009.03.003 PMID: 19323993

82. Rivera C, Voipio J, Kaila K (2005) Two developmental switches in GABAergic signalling: the K+-Cl-cotransporter KCC2 and carbonic anhydrase CAVII. J Physiol 562: 27–36. PMID: 15528236

83. Raimondo JV, Markram H, Akerman CJ (2012) Short-term ionic plasticity at GABAergic synapses. Front Synaptic Neurosci 4: 5. doi: 10.3389/fnsyn.2012.00005 PMID: 23087642

84. Qian Z, Micorescu M, Yakhnitsa V, Barmack NH (2012) Climbing fiber activity reduces 14-3-3-theta regulated GABA(A) receptor phosphorylation in cerebellar Purkinje cells. Neuroscience 201: 34–45. doi: 10.1016/j.neuroscience.2011.11.021 PMID: 22119642

85. Brenowitz SD, Regehr WG (2005) Associative short-term synaptic plasticity mediated by endocannabinoids. Neuron 45: 419–431. PMID: 15694328

86. Marandi N, Konnerth A, Garaschuk O (2002) Two-photon chloride imaging in neurons of brain slices. Pflugers Arch 445: 357–365. PMID: 12466938

87. Kaila K, Price TJ, Payne JA, Puskarjov M, Voipio J (2014) Cation-chloride cotransporters in neuronal development, plasticity and disease. Nat Rev Neurosci 15: 637–654. doi: 10.1038/nrn3819 PMID: 25234263

88. Jedlicka P, Deller T, Gutkin BS, Backus KH (2011) Activity-dependent intracellular chloride accumulation and diffusion controls GABA(A) receptor-mediated synaptic transmission. Hippocampus 21: 885–898. doi: 10.1002/hipo.20804 PMID: 20575006

89. Berglund K, Schleich W, Wang H, Feng G, Hall WC, Kuner T, et al. (2008) Imaging synaptic inhibition throughout the brain via genetically targeted Clomeleon. Brain Cell Biol 36: 101–118. doi: 10.1007/s11068-008-9031-x PMID: 18850274

90. Bregestovski P, Waseem T, Mukhtarov M (2009) Genetically encoded optical sensors for monitoring of intracellular chloride and chloride-selective channel activity. Front Mol Neurosci 2: 15. doi: 10.3389/neuro.02.015.2009 PMID: 20057911

91. Kuner T, Augustine GJ (2000) A genetically encoded ratiometric indicator for chloride: capturing chloride transients in cultured hippocampal neurons. Neuron 27: 447–459. PMID: 11055428

92. Isomura Y, Sugimoto M, Fujiwara-Tsukamoto Y, Yamamoto-Muraki S, Yamada J, Fukuda A (2003) Synaptically activated Cl- accumulation responsible for depolarizing GABAergic responses in mature hippocampal neurons. J Neurophysiol 90: 2752–2756. PMID: 14534278

93. Staley KJ, Soldo BL, Proctor WR (1995) Ionic mechanisms of neuronal excitation by inhibitory GABAA receptors. Science 269: 977–981. PMID: 7638623

94. Mercer AJ, Rabl K, Riccardi GE, Brecha NC, Stella SL Jr., Thoreson WB (2011) Location of release sites and calcium-activated chloride channels relative to calcium channels at the photoreceptor ribbon synapse. J Neurophysiol 105: 321–335. doi: 10.1152/jn.00332.2010 PMID: 21084687

95. Peters CJ, Yu H, Tien J, Jan YN, Li M, Jan LY (2015) Four basic residues critical for the ion selectivity and pore blocker sensitivity of TMEM16A calcium-activated chloride channels. Proc Natl Acad Sci U S A. 112: 3547–3552. doi: 10.1073/pnas.1502291112 PMID: 25733897